

Controls on Bending-Related Faulting Offshore of the Alaska Peninsula

Jacob Clarke¹, Donna Shillington², Regalla Christine², James B. Gaherty², Justin Estep², Douglas A Wiens³, Anne Bécel⁴, and Mladen R. Nedimovic⁵

¹Southern Methodist University

²Northern Arizona University

³Washington University

⁴Lamont-Doherty Earth Observatory

⁵Dalhousie University

October 17, 2023

Abstract

Oceanic plates experience extensive normal faulting as they bend and subduct, enabling fracturing of the crust and upper mantle. Debate remains about the relative importance of pre-existing faults, plate curvature and other factors in controlling the extent and style of bending-related faulting. The subduction zone off the Alaska Peninsula is an ideal place to investigate controls on bending-related faulting as the orientation of abyssal-hill fabric with respect to the trench and plate curvature vary along the margin. Here we characterize bending faulting between longitudes 161°W and 155°W using newly collected multibeam bathymetry data. We also use a compilation of seismic reflection data to constrain patterns of sediment thickness on the incoming plate. Although sediment thickness increases by over 1 km from 156°W to 160°W, most sediments were deposited prior to the onset of bending faulting and thus have limited impact on the expression of bend-related fault strikes and throws in bathymetry data. Where magnetic anomalies trend subparallel to the trench (<30°) west of ~156°W, bending faulting parallels magnetic anomalies, implying bending faulting reactivates pre-existing structures. Where magnetic anomalies are highly oblique (>30°) to the trench east of 156°W, no bending faulting is observed. Summed fault throws increase to the west, including where pre-existing structure orientations do not vary between 157-161°W, suggesting that the increase in slab curvature directly influences fault throws. However, the westward increase in summed fault throws is more abrupt than expected for changes in slab bending alone, suggesting potential feedbacks between pre-existing structures, slab dip, and faulting.

Hosted file

975476_0_art_file_11439992_s1rmx7.docx available at <https://authorea.com/users/670587/articles/670495-controls-on-bending-related-faulting-offshore-of-the-alaska-peninsula>

Hosted file

975476_0_supp_11439996_s1rmx7.docx available at <https://authorea.com/users/670587/articles/670495-controls-on-bending-related-faulting-offshore-of-the-alaska-peninsula>

Controls on Bending-Related Faulting Offshore of the Alaska Peninsula

Jacob Clarke^{1,2}; Donna J. Shillington¹, Christine Regalla¹; James B. Gaherty¹; Justin Estep¹,
Douglas A. Wiens³, Anne Bécél⁴, Mladen R. Nedimović⁵

¹Northern Arizona University, School of Earth and Sustainability, Flagstaff, AZ USA

²Southern Methodist University, Dallas, TX, USA

³Washington University in St Louis, St Louis, MO USA

⁴Lamont-Doherty Earth Observatory of Columbia University, Palisades, NY USA

⁵Dalhousie University, Halifax, NS, Canada

Corresponding author: Jacob Clarke

Key Points:

- Bathymetry data reveal variations in the orientation and amount of bending faulting outboard of the Alaska subduction zone
- The westward increase in bending faulting is due to a combination of favorably oriented pre-existing structures and increased slab dip
- Variable bending faulting and volcanic constructs updip of 2020 M7.6 intraplate earthquake implies complex stress state in subducting slab

Abstract

Oceanic plates experience extensive normal faulting as they bend and subduct, enabling fracturing of the crust and upper mantle. Debate remains about the relative importance of pre-existing faults, plate curvature and other factors in controlling the extent and style of bending-related faulting. The subduction zone off the Alaska Peninsula is an ideal place to investigate controls on bending-related faulting as the orientation of abyssal-hill fabric with respect to the trench and plate curvature vary along the margin. Here we characterize bending faulting between longitudes 161°W and 155°W using newly collected multibeam bathymetry data. We also use a compilation of seismic reflection data to constrain patterns of sediment thickness on the incoming plate. Although sediment thickness increases by over 1 km from 156°W to 160°W, most sediments were deposited prior to the onset of bending faulting and thus have limited impact on the expression of bend-related fault strikes and throws in bathymetry data. Where magnetic anomalies trend subparallel to the trench ($<30^\circ$) west of $\sim 156^\circ\text{W}$, bending faulting parallels magnetic anomalies, implying bending faulting reactivates pre-existing structures. Where magnetic anomalies are highly oblique ($>30^\circ$) to the trench east of 156°W , no bending faulting is observed. Summed fault throws increase to the west, including where pre-existing structure orientations do not vary between $157\text{--}161^\circ\text{W}$, suggesting that the increase in slab curvature directly influences fault throws. However, the westward increase in summed fault throws is more abrupt than expected for changes in slab bending alone, suggesting potential feedbacks between pre-existing structures, slab dip, and faulting.

43 **Plain Language Summary**

44 Subduction zones are plate boundaries where two tectonic plates converge, and the oceanic plate
45 is bent and forced to below the other plate. Oceanic plates are faulted as they bend, and these
46 “bending faults” are thought to be important for controlling the deep water cycle on Earth and
47 influencing the generation of large earthquakes in subduction zones. The amount and style of
48 bending faulting varies between and within subduction zones around the world, and debate
49 remains about what causes this variability. Possible controls include the overall curvature of the
50 oceanic plate as it bends and subducts and pre-existing weaknesses in the oceanic plate from
51 when it formed. We use bathymetry data across the Alaska subduction zone to characterize
52 bending faults here and understand controls on their formation. This is an ideal study area
53 because the curvature of the plate and the pre-existing weaknesses vary in this region. The
54 amount of bending faulting increases abruptly to the west and appears to result from a feedback
55 between favorably oriented pre-existing weaknesses and increased curvature of the oceanic plate.
56 These results can be used to understanding bending faulting in other subduction zones.

1 Introduction

Bending and loading of the subducting oceanic lithosphere at subduction zones causes the crust and upper mantle to flex, forming a bulge seaward of the trench that has been termed the outer rise (Bodine & Watts, 1979; Caldwell et al., 1976; Garcia et al., 2019). Flexure of the incoming plate and negative buoyancy of the downwelling slab puts the upper portion of the lithosphere under extension and results in normal faulting in the incoming plate (Chapple & Forsyth, 1979; Faccenda, 2014; Ranero et al., 2003). These normal faults, known as bending-related faults, are found at subduction zones around the globe and occur between the trench axis and outer-rise in a region termed the outer trench slope (Hilde, 1983; Masson, 1991).

Faulting of downgoing slabs prior to subduction is thought to have several influences on subduction processes: 1) faults provide pathways for seawater infiltration into and hydration of the oceanic lithosphere (Cai et al., 2018; Contreras-Reyes et al., 2008; Faccenda, 2014; Fujie et al., 2018; Hacker, 2008; Van Keken et al., 2011; Wei et al., 2021); 2) bending-related faulting contributes to frictional heterogeneity on the megathrust once subducted (Wang & Bilek, 2014); and 3) faults host normal-faulting earthquakes both outboard and within the subduction zone (Lay et al., 2009, 2011; Ranero et al., 2005). Water has been interpreted to be stored in the upper mantle of the downgoing plate (e.g., Cai et al., 2018; Grevemeyer et al., 2018; Ivandic et al., 2008; Lefeldt et al., 2012; Ranero et al., 2003; Shillington et al., 2015) in the form of serpentinite, the hydrous alteration of peridotite in the upper mantle. Water can also be stored as pore fluids in fault zones in the crust and mantle of the incoming plate, and contained in seafloor sediments (Canales et al., 2017; Faccenda, 2014; Iyer et al., 2012; Miller et al., 2021). The breakdown of serpentinite and release of water at depth could influence pore fluid pressures

along the megathrust interface (Hasegawa & Nakajima, 2017; Peacock, 2001), the volume and composition of arc magmatism (e.g., Wei et al., 2021), and the occurrence of intermediate depth earthquakes (Boneh et al., 2019; Kita et al., 2006; Ranero et al., 2005; Shillington et al., 2015; Wei et al., 2021). Therefore, better knowledge on the controls on bending-related faulting formation, fault throws, and lateral extent can lead to further understanding of the subduction water cycle, earthquakes, and magmatism.

Although the existence of these faults at subduction zones is well documented, the style and magnitude of faulting vary between and within subduction zones (e.g., Contreras-Reyes et al., 2008; Eimer et al., 2020; Fujie et al., 2018; Kobayashi et al., 1995, 1998; Obana et al., 2019; Ogawa et al., 1997; Ranero et al., 2003; Van Avendonk et al., 2011). Thus, questions remain on the primary controls on bending faulting. Possible controls include plate curvature (Naliboff et al., 2013; Nishikawa & Ide, 2015), plate age (Protti et al., 1994), and/or pre-existing structures (Fujie et al., 2018; Ranero et al., 2003; Shillington et al., 2015). The curvature of the slab is correlated with the elastic thickness of the plate, which is largely determined by the slab age and temperature (Bodine & Watts, 1979; Pérez-Gussinyé et al., 2008). Additionally, fracturing due to bending of the downwelling slab and resulting serpentinization of the upper mantle may weaken the slab, allowing for more bending and hence further faulting (Contreras-Reyes & Osses, 2010).

In this study, we use a compilation of multibeam bathymetry data, including recently acquired data from the Alaska Amphibious Community Seismic Experiment (AACSE) in 2018-2019 (Barcheck et al., 2020), to characterize bending-related faults in detail, including orientations, lengths, spacing, and scarp heights. To test models for controls on faulting, we compare these

bending-fault characteristics with the orientations of pre-existing abyssal-hill faults from magnetic data, orientation of the trench, and changes in dip of the incoming plate along strike.

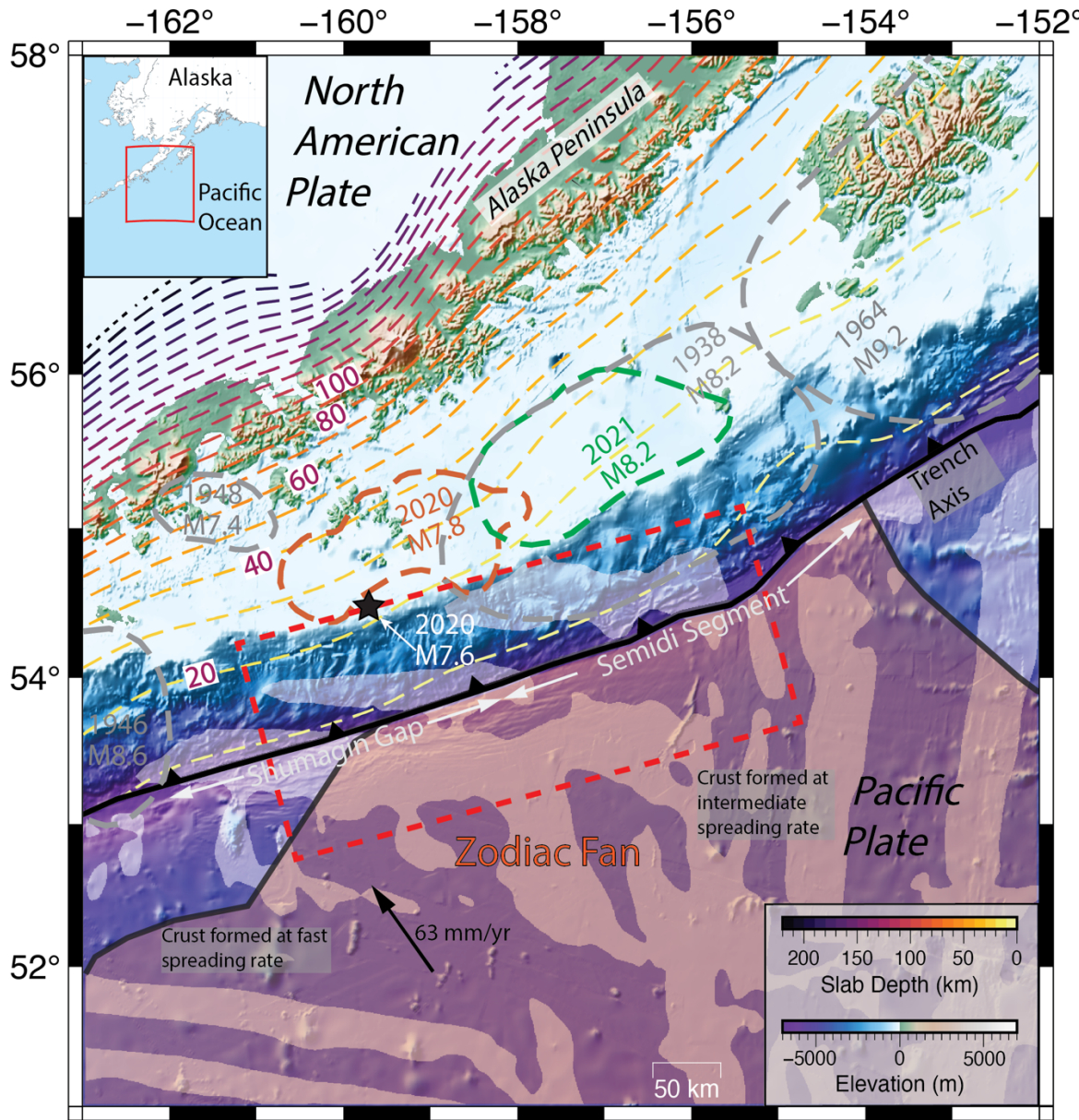


Figure 1: Map of study area with historic large rupture zones (gray dotted outlines, Davies et al., 1981), 2020 M7.8 rupture (orange dotted outline, Xiao et al., 2021), 2021 M8.2 Chignik rupture (green dotted outline, Elliot et al., 2022), 2020 M7.6 intraplate event centroid (black star), trench axis (solid barbed black line, Basset & Watts, 2015), magnetic anomalies (positive anomalies shown with white patches on incoming Pacific plate, Maus et al., 2009) slab depth contours (colored dotted lines – 10 km contours, Hayes et al., 2018), and sediments derived from the Zodiac

Fan (orange shaded area, von Huene et al., 2012). Primary study area with new high-resolution bathymetry data (dashed red box) between longitudes 155-161°W. Convergence rate from Sella et al., (2002) shown with black arrow and text. Inset shows study area location.

2 Tectonic Background

The subduction zone offshore of the Alaska Peninsula is an ideal location to examine controls on the formation of bending-related faulting (Fig. 1). The subducting plate has an age of ~55 Ma throughout the study area (Lonsdale et al., 1988) and is subducting nearly orthogonally at a rate of 63 mm/yr (Sella et al., 2002). The strike of the trench axis also remains relatively uniform at an azimuth of ~70° through the study area, which spans longitudes 155-161°W. The consistent plate age, trench axis strike, and convergence rate leads to a nearly constant thermal structure of the subduction zone.

Although the age and convergence direction are constant, the dip of the slab and orientation of pre-existing structures vary along strike. The dip of the slab steepens from the Gulf of Alaska west to the Aleutians, including steepening between the eastern Semidi segment, longitudes ~155-159°W, and the western Shumagin Gap, longitudes ~159-162°W (Hayes et al., 2018; Kuehn, 2019; Fig. 1). One possible cause for the eastward shallowing of the slab is the subduction of an oceanic plateau (the Yakutat block) in the easternmost part of Alaska subduction zone; the buoyancy resulting from the thickened crust is thought to contribute to shallow slab subduction there (Worthington et al., 2012). Another possible cause for westward increase in the slab dip is a transition from oceanic/continental subduction to oceanic/oceanic subduction; west of the primary study region, the subduction zone transitions to an

oceanic/oceanic margin which may promote slab steepening (Holt et al., 2015; Sharples et al., 2014).

The spreading history of the incoming oceanic crust also varies along strike, separated by a remnant triple junction marking the relict Kula, Pacific, Farallon triple junction (Engebretson et al., 1985; Lonsdale, 1988). The remnant triple junction appears as a T-shaped feature in the magnetic data at $\sim 158^\circ\text{W}$ (Fig. 1). Cessation of spreading at this triple junction occurred between $\sim 43\text{--}44$ Ma (Engebretson et al., 1985; Lonsdale, 1988). Oceanic crust formed from Kula-Pacific spreading is currently subducting in the Shumagin Gap ($\sim 159\text{--}162^\circ\text{W}$) and western Semidi segment ($\sim 155\text{--}159^\circ\text{W}$). This crust formed at fast spreading rates (half rates of ~ 74 mm/yr, Engebretson et al., 1985), and magnetic anomalies trend slightly oblique to the trench axis by $\sim 20^\circ$. Oceanic crust in the eastern Semidi segment formed from Pacific-Farallon spreading at intermediate rates (half rates of $\sim 28\text{--}34$ mm/yr, Engebretson et al., 1985). Magnetic anomalies in this crust trend highly oblique to the trench ($\sim 70^\circ$). Tectonic reconstructions by Fuston & Wu (2020) suggest the possible existence of a Resurrection plate and Kula-Resurrection ridge striking N-S that would have subducted beneath the Alaska Peninsula. The proposed Kula-Resurrection ridge would have been active from $\sim 60\text{--}40$ Ma.

Previous work, based on lower-resolution bathymetry data along the Alaska-Aleutian trench largely focused on a region further west than our primary study area, identified a connection between the trends of magnetic anomalies and strikes of bending-related faults (Masson, 1991; Mortera-Gutiérrez et al., 2003). Masson (1991) showed the angle between pre-existing abyssal hills inferred from magnetic anomalies plays a key role in whether bending reactivates abyssal-

hills or forms new faults, including in the Alaska-Aleutian subduction. In the western Aleutians, between 179°E and 169°W, analysis of bathymetry data shows that fault strikes closely follow the oceanic spreading fabric which is near parallel to the trench (<10° difference) (Masson, 1991; Mortera-Gutiérrez et al., 2003). Between 157°W and 169°W, bending faults show two strikes: one primary set following the inherited spreading fabric, and a secondary set parallel to the trench axis (Masson, 1991). The angle between the trench and abyssal-hill faults is up to 30° in that region, and bending fault orientations suggest both reactivation of inherited weaknesses and the formation of new bending faults paralleling the trench.

Shillington et al. (2015) used 2D active-source seismic transects to show that the incoming plate outboard of the Shumagin Gap (~159-162°W) is more pervasively faulted than the Semidi segment (~155-159°W). They also found that the upper mantle of the slab has a larger area of reduced seismic velocities seaward of the Shumagin Gap compared to the Semidi segment, which they attributed to an increase in hydration and associated serpentinization to the west. The Shumagin Gap also has a higher amount of seismicity in the outer rise, which could suggest a greater number of bending-related faults (Shillington et al., 2015).

In addition to possible along-strike changes in bending faulting and resulting hydration, the Alaska peninsula also exhibits changes in coupling (Drooff & Freymueller, 2021; Li & Freymueller, 2018), great earthquake history (Davies et al., 1981), seismicity at a range of depths (Shillington et al., 2015; Wei et al., 2021), and arc chemistry (Buurman et al., 2014; Wei et al., 2021), all of which have been proposed to be influenced by faulting and hydration of the incoming plate. The Semidi segment has a history of generating great ($M > 8.0$) earthquakes with

a recurrence interval of ~50-75 years (Davies et al., 1981), including the recent M8.2 Chignik earthquake in July 2021 in the western part of the Semidi segment (e.g., Elliott et al., 2022; Liu et al., 2022). GPS measurements show that the Semidi segment is highly locked overall and that locking increases to the east (Drooff & Freymueller, 2021; Li & Freymueller, 2018; Zhao et al., 2022). The Shumagin Gap, however, is only weakly coupled (<30% coupled). Great earthquakes along the megathrust appear to be less common in the Shumagin Gap, with the last occurring in 1847 or possibly 1788 (Davies et al., 1981). However, the eastern part of the deep Shumagin Gap did recently rupture in a M7.8 earthquake in July 2020 (Liu et al., 2022; Xiao et al., 2021) and hosted an intraplate M7.6 earthquake in October 2020 (Zhou et al., 2022). Greater roughness at the top of the subducting plate due to increased bending faulting (e.g., Li et al., 2018; Wang & Bilek, 2014) and fluids from the hydrated lithosphere (Li & Freymueller, 2019) have been proposed to contribute to changes in locking and earthquake history.

There are also along-strike changes in intermediate depth earthquakes (Shillington et al., 2015) and calculated *b*-values (Wei et al., 2021). Florez & Prieto (2019) showed that subduction zones with high *b*-values (a comparatively greater ratio of small earthquakes to large earthquakes) suggest greater extent of dehydration reaction, and thus more water stored in the downgoing plate. The Semidi segment is characterized by a double-seismic zone with moderate *b*-values and few earthquakes extending deeper than 100 km (Abers, 1992; Wei et al., 2021). This suggests that the volume of water stored in the downgoing slab through bending faults at this segment is less than other subduction segments to the west. High *b*-value earthquakes in the Shumagin Gap extend to depths >200 km, implying greater amounts of water stored here (Wei et al., 2021). Finally, trace element geochemistry at volcanic centers in the Shumagin and Semidi segments

show that sediment input of source magmas is higher at the Semidi segment and water input is less (Wei et al., 2021).

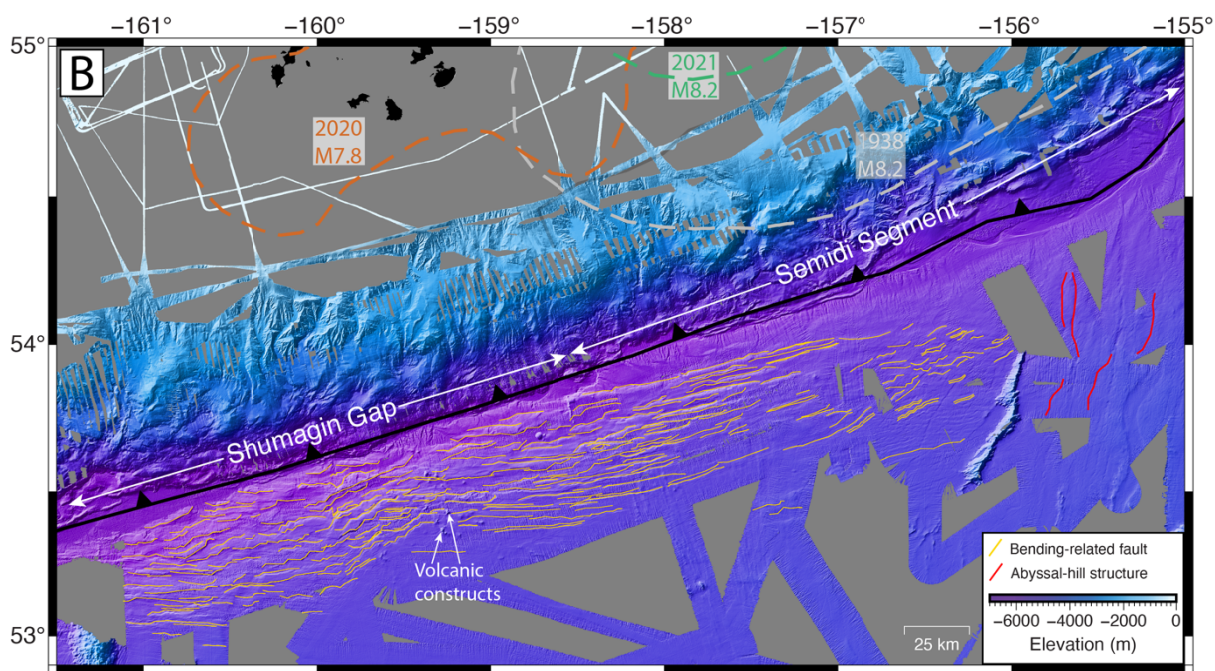
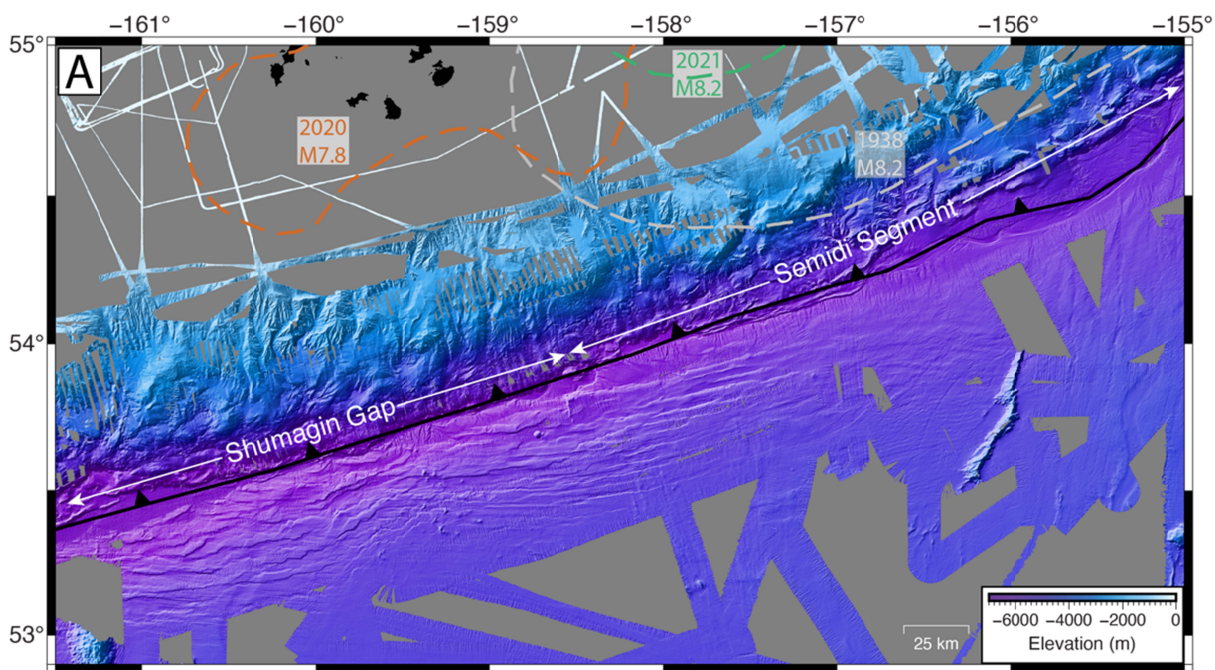
3 Data and Methods

We map and characterize bending faults on the incoming plate offshore of the Alaska Peninsula using a compilation of existing bathymetry data. Recently deposited sediments have the potential to mask the bathymetric expression of bending faults, so where it is available, we use existing seismic reflection data to map the total sediment thickness and thickness of trench fill deposited during bending faulting. Finally, to examine possible controls on bending-related faulting, we use the trends of magnetic anomalies to estimate the strike of pre-existing faults and fractures, and calculate the dip of the incoming plate outboard of the trench.

3.1 Characterizing bending faulting in bathymetry data

We map bending-related faults between longitudes 161-155°W (Fig. 2) using new high-resolution multibeam bathymetry data collected as part of AACSE (Barcheck et al., 2020; Bécél et al., 2019) combined with other existing bathymetric data (Ryan et al., 2009; Fig. 2). The combined data provide nearly complete, continuous coverage of an area spanning roughly 100x300 km with a 125-m grid resolution, forming an excellent basis for systematic identification and characterization (geometry and displacement) of faults based on their surface expression. While bathymetry data are limited due to their inability to quantify faults in the subsurface, the seismic datasets that enable subsurface quantification of faults (section 3.3) are too incomplete to allow for a comprehensive characterization of the entire region. The mapped region encompasses the incoming plate subducting in the Shumagin Gap (159-162°W) and Semidi segment (155-159°W). Previous efforts to examine bending faults offshore of the Alaska

225 Peninsula used lower resolution (~200 m) GLORIA and Seabeam swath data (Scanlon &
226 Masson, 1992) or spatially limited swath data from modern sonar systems (Shillington et al.,
227 2015). The availability of new high-resolution bathymetry area provides the opportunity to map
228 faults in greater detail and extent. Faults are mapped by hand using a processed bathymetry grid
229 that is detrended and demeaned to produce relative elevation, which removes long-wavelength
230 variations and highlights faulting (Fig. 2, Supplementary Fig S-8). Detrending is done by
231 applying a cosine bandpass filter with corners at 10000/3000/1000/100 m. These values have
232 been chosen based on the average and minimum spacings between bending-related faults. Only
233 faults with minimum scarps of ± 5 m in the detrended grid are included in this mapping effort.



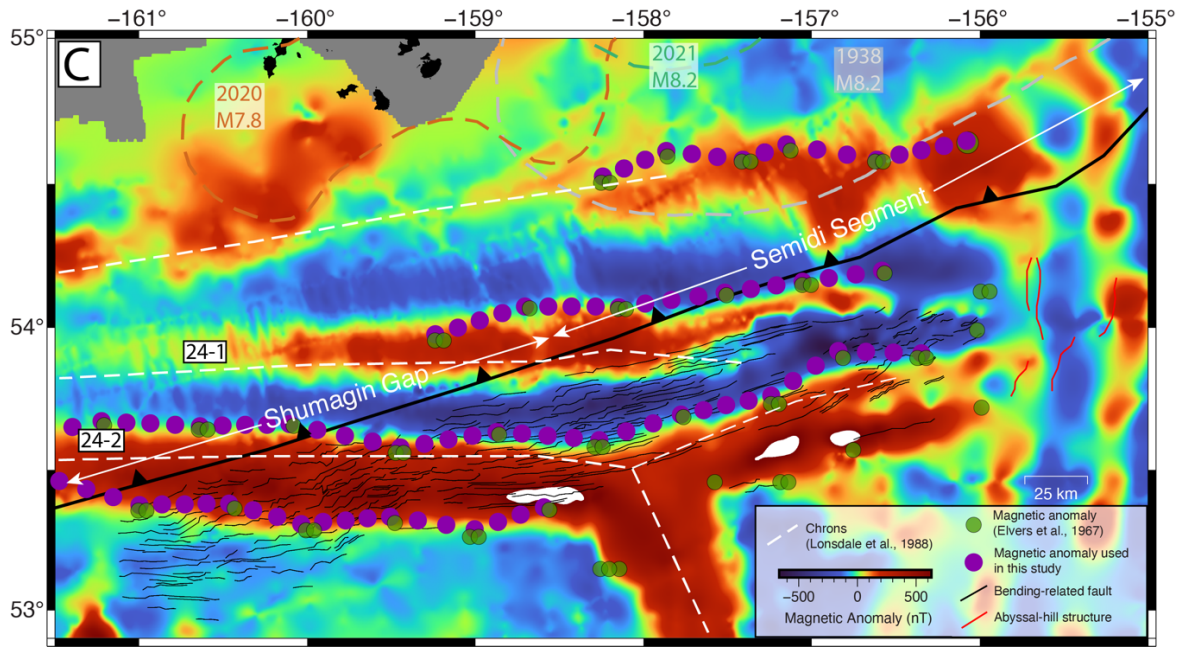


Figure 2: A) New high-resolution bathymetry data (Barcheck et al., 2020; Ryan et al., 2009). Gray areas show regions without swath bathymetry coverage. The trench axis (Basset & Watts, 2015) is shown by the thick black line in all panels. B) Interpreted bathymetry data with mapped bending-related faults (yellow). Red lines in the eastern part of the study area that are oriented N-S may show interpreted remnant abyssal-hill structures and not active bending-related faults. Rupture patches are shown on the overriding plate with colors matching those shown in Figure 1. C) Mapped bending-related faults (thin black lines) overlain on magnetic anomaly grid (Bankey et al., 2002). Note the rotation in spreading direction from N-S west of $\sim 156^{\circ}\text{W}$ to E-W east of $\sim 156^{\circ}\text{W}$. White dashed lines and boxed annotations show magnetic chrons based on interpretations from Lonsdale et al. (1988). A remnant triple junction can be observed at 158°W . Green dots show magnetic anomaly picks from Elvers et al. (1967) used as a guide for magnetic anomaly picks presented in this study (larger purple points). Notice the apparent absence of bending faults at the seafloor east of $\sim 156^{\circ}\text{W}$ (and not at the triple junction), where orientations of magnetic anomalies change. Magnetic anomaly orientations do not change at the triple junction due to a plate reorganization that occurred ~ 53 Ma (Lonsdale, 1988).

Each mapped fault trace is resampled to 100 m intervals along-strike. We measure fault strike, fault dip direction (seaward or trenchward), and distance from the trench for each 100 m

segment. We examine variations in bending fault strike along the subduction zone by calculated histograms of fault azimuth in 1° wide bins (Fig. 3).

The maximum throw for each fault is estimated using a profile extracted orthogonal to the portion of the fault that has the largest difference in maximum and minimum elevations in the detrended bathymetry grid. Surfaces and 95% confidence intervals for the hanging wall, footwall and fault plane are estimated through linear regression using hand-picked points from the bathymetric profile. These surfaces are then used to calculate the vertical separation, heave and throw assuming a dip of 60° (Figs. S-1, S-2). To examine along-strike variations in the total amount of fault slip, maximum throw estimates are summed within 0.5° wide bins.

3.2 Estimating orientations of pre-existing structures from magnetic anomaly data

Inherited abyssal-hill fabric within oceanic plates can be estimated from magnetic anomalies, where abyssal-hill faults are expected to form parallel to the mid-ocean ridge due to normal faulting (e.g., Macdonald et al., 1996), and thus parallel to the trend of magnetic anomalies. Elvers et al. (1967) map isochrons in detail on the subducting Pacific plate in our study area. To estimate the likely orientation of pre-existing faults in our study area, we resample picks made by Elvers et al. (1967) (which closely follows magnetic anomaly peaks of the North American magnetic anomaly map created by Bankey et al. (2002)) to 1 km. Based on these magnetic anomaly picks, we estimate the strikes and standard deviations of abyssal-hill faults that may be reactivated during slab bending in 1° wide bins using four distinct anomalies in the study area (Figs. 2C, 3).

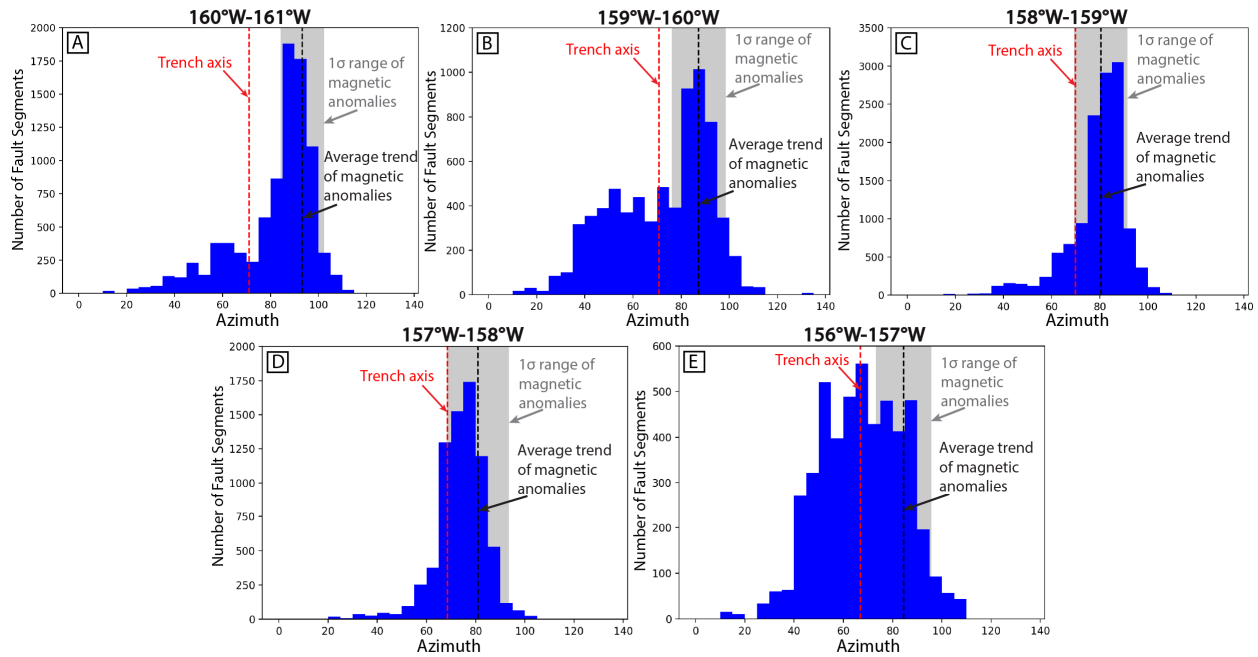


Figure 3: Histograms comparing fault segment strike azimuths (blue bars) in 1-degree bins with the average trend of the trench (red dotted line, Bassett & Watts, 2015) and average trend of magnetic anomalies (black dotted line). One-standard-deviation range of magnetic anomalies is shown by the gray box in the background. Dominant peaks of fault strikes primarily follow the trend of magnetic anomalies (panels A, C, D). Between 159-160°W (panel B), fault strike azimuths show one dominant trend following magnetic anomalies, and a secondary trend ranging from ~35-80°. Between 156-157°W, there are fewer faults with a broader distribution of strike azimuths (panel E). Note that vertical axis varies between panels.

3.3 Sediment thickness and basement offsets from seismic reflection data

We compile seismic reflection data collected on the incoming plate from the National Archive of Marine Seismic Surveys (NAMSS, Triezenberg et al., 2016), the ALEUT experiment (Bécel et al., 2015, 2017; Kuehn, 2019; Li et al., 2015) and the AACSE experiment (Barcheck et al., 2020; Bécel et al., 2019) to determine total sediment thickness and the thickness of sediments within the trench throughout the study area (Fig. 4). Previous studies have documented along-strike changes in sediment thickness on the incoming plate, with larger sediment thickness offshore of

291 the Semidi segment (Straume et al., 2019). The thickness of trench fill sediments also varies
292 along the margin (e.g., von Huene et al., 2012), and this portion of the sedimentary section has
293 the highest potential to mask bending faults because it was deposited during the time of bending
294 fault formation and development. We pick arrival times for the seafloor, base of trench fill, and
295 top of igneous crust on time migrated profiles (Fig. 5). Subtracting the seafloor from the base of
296 trench fill and from the top of igneous crust provides thickness in two-way travel time of the
297 trench fill and total sediment section, respectively. We convert time to depth using a velocity of
298 1.8 km/s; this average velocity is based on seismic processing of ALEUT reflection data (Bécel
299 et al., 2015). We use a single velocity for depth conversion due to uncertainty in both spatial
300 distribution and depth-dependent velocities for each of the three sediment packages on the
301 incoming plate: pelagic sediments, terrigenous fan sediments, and Quaternary trench fill
302 (Creager et al., 1973; Stevenson et al., 1983; von Huene et al., 2012). These uncertainties obviate
303 the benefit of using a depth-dependent velocity for conversion. To create a grid of total sediment
304 thickness and trench fill on the incoming Pacific plate, we grid the resulting sediment thickness
305 values using a nearest neighbor algorithm with a 100-km radius and 0.1° grid spacing (Fig 4).

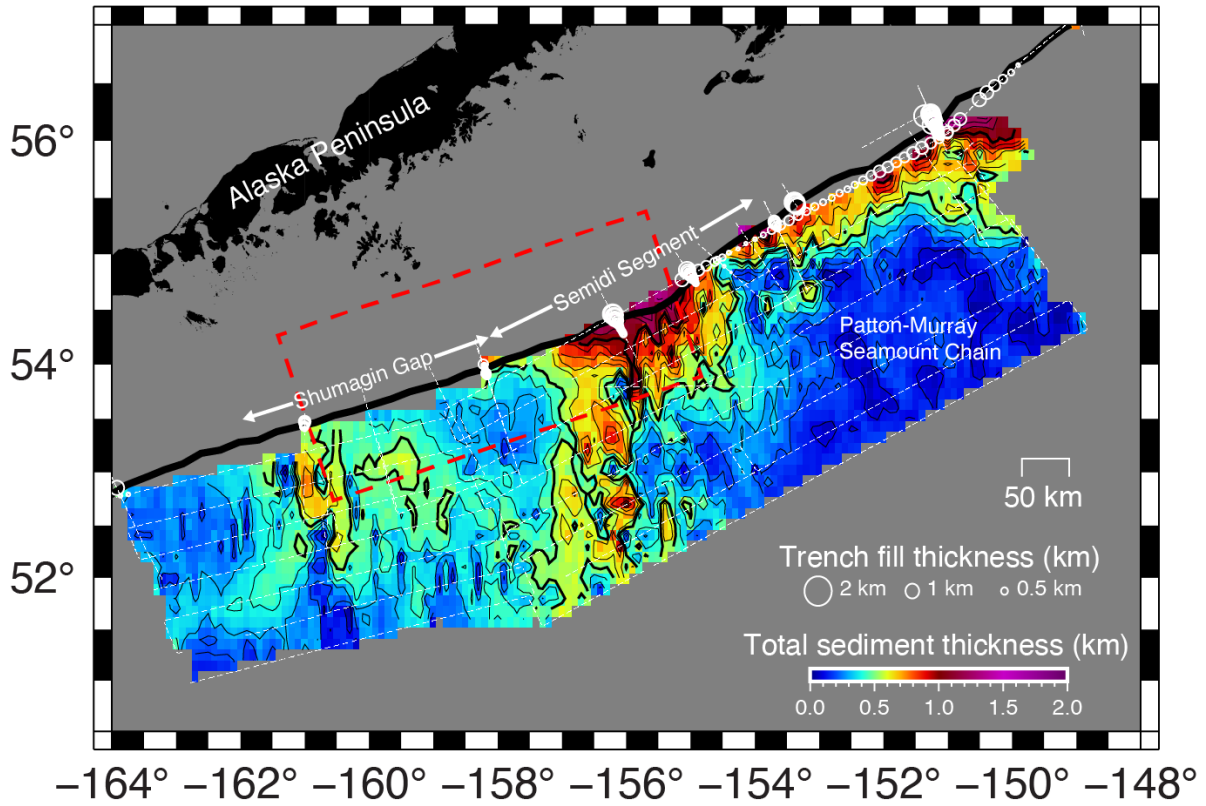


Figure 4: Map of gridded sediment thickness based on legacy single-channel USGS seismic reflection lines (Triezenberg et al., 2016) and multi-channel seismic reflection lines from ALEUT (Bécel et al., 2015, 2017; Kuehn, 2019; Li et al., 2015) and AACSE (Bécel et al. 2019). Seismic profiles shown with dashed white lines. The thickness of trench fill indicated with open circles sized by thickness. The absence of a trench fill circle for trench-perpendicular lines represents a thickness of zero. Primary study area shown by dashed red box as in Fig. 1.

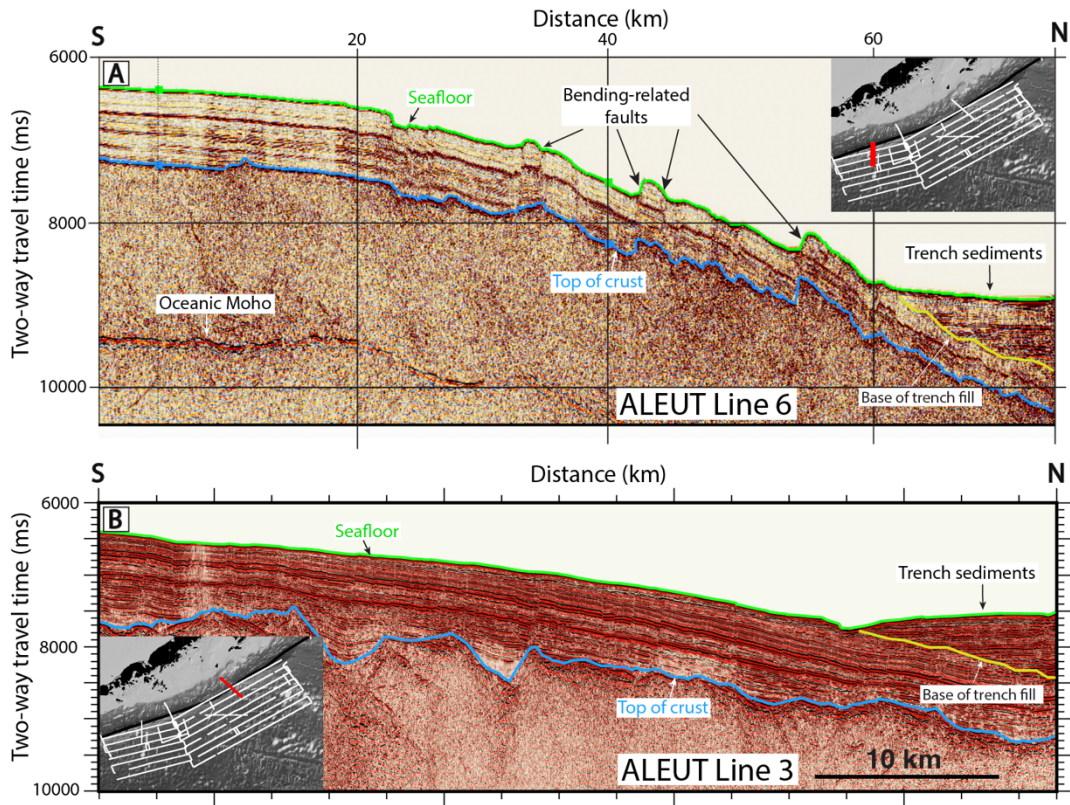


Figure 5: Examples of seismic reflection profiles A) outboard of the Shumagin Gap (ALEUT line 6) showing extensive bending faulting at the seafloor and top of the crust (Bécel et al., 2017) and B) Outboard of the Semidi Segment, with few to no bending fault expressions in the sediments or at the top of the crust (Shillington et al., 2015). Insets show seismic line locations highlighted in red. Topography in the top of crust outboard of the Semidi segment (panel B) is largely caused by the formation of crust at moderate spreading rates, which creates a more faulted crust surface at formation than fast spreading rates offshore of the Shumagin Gap, and these features are likely not active bending-faulting. There is little evidence of faulting-caused deformation in the sediments in this region and observable deformation may be caused by differential compaction.

3.4 Estimating bending angle from bathymetry data and seismic reflection profiles

The dip of the slab at depth increases along strike (e.g., Hayes et al., 2018; Kuehn, 2019), and we seek to evaluate the contribution of changes in slab bending to observed patterns of faulting. We create a grid of the depth to top of igneous crust by subtracting the grid of sediment thickness

326 described in section 3.3 from the bathymetry grid. We calculate the dip of the incoming plate
327 near the trench by applying linear regression of 50-km-long trench-perpendicular profiles of the
328 top of igneous crust (Fig. 6) following the method of Nishikawa & Ide (2015). For comparison,
329 we also estimate dip of the seafloor along the same profiles using the same bathymetry data as
330 the fault mapping analysis (Figs. 7, S-6).

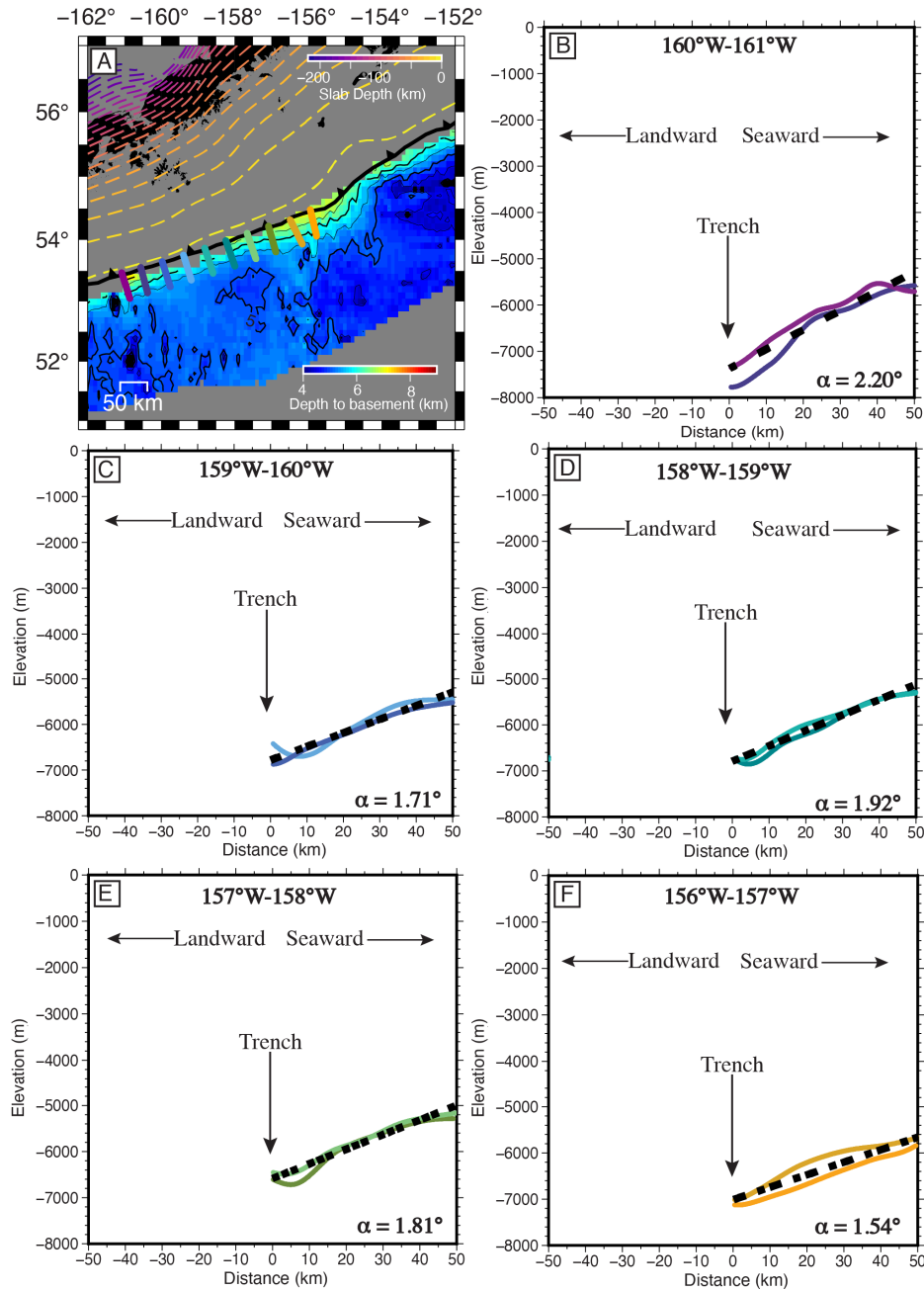


Figure 6: A) Regional map showing the locations of profiles used to estimate outer rise dip outboard of the trench and grid of depth to basement based on bathymetry data (Fig. 1) and sediment thickness (Fig. 4). Colored trench-perpendicular profiles match those in B-F. B-F). Linear regressions (black dashed lines) through two bathymetric profiles (colored lines, see panel A for location) ~ 0.5 degrees apart. Dip angles (alpha) for each longitudinal bin labeled on plot. For comparison, we also estimated dip of the incoming plate at the seafloor (Fig. S-6), which shows a general westward increase in slab dip.

4 Results

We interpret 255 bending-related faults offshore of the Alaska Peninsula between longitudes 161°W and 155°W. Bending faulting is observed progressively farther from the trench outboard of the eastern Semidi segment compared to outboard the western Shumagin segment. In the western part of the study area (west of 158°W), most bending faults are concentrated within 50 km of the trench, but farther east faults are observed up to 75 km from trench (Figs. 2, S-3). We do not observe any active bending-faults east of 156°W in the newly acquired bathymetry data; all the potential structures that can be mapped here are oriented roughly N-S (Fig. 2B) and likely represent differential compaction over relict abyssal-hill spreading faults or associated structures.

Individual mapped faults have lengths of ~10-20 km, are spaced ~ 3 km apart, and have maximum estimated throws of up to 423 m. Fault length varies along the trench, with average lengths of 15.6 km, 13.9 km, 20.6 km, 19.7 km, and 10.6 km, in 1° bins from 161°W to 156°W. There are similar numbers of faults dipping toward the trench and away from the trench. However, faults that dip trenchward generally exhibit larger scarp heights than those dipping seaward (Fig. S-3). Cumulative fault throw summed across all mapped faults increases markedly from east to west, with the eastern portion having both fewer total number of faults and smaller estimated fault throws than the west (Fig. 7).

A comparison of bending fault azimuths with the orientations of the trench and magnetic anomalies shows that bending faults generally parallel pre-existing structures (Fig. 3). Bending-related faults in our study area primarily have strike azimuths between 80-100° (Fig. 3). West of 157.5°W, magnetic anomalies parallel inferred abyssal-hill faults, which dominantly strike E-W

(azimuths of 80-90°). Here faults strike 10-20° oblique to the trench axis which has a relatively uniform azimuth of ~70° (Figs. 2C, 3). Between 157.5 and 156°W, magnetic anomalies are less continuous, and their orientations rotate to ENE-WSW, nearly parallel to the trench axis. East of 156°W, magnetic anomalies strike ~N-S and no bending faults are observed.

There are two key areas where fault strikes are not subparallel to magnetic anomaly trends. The first is at ~159.25-160°W, where bending fault strikes show one dominant trend centered at ~85° and a broad secondary trend ranging from ~35-80°. This area also contains small mounds (Fig. 2B) that we tentatively interpret as petit spot volcanic constructs due to their morphological similarity to petit spot volcanoes found at other subduction zones, such as the Japan trench (Hirano, 2011; Hirano et al., 2006). The second is located between 156-157°W where fault strike azimuths span a wide range from ~35-100° (Figure 3). This region is just west of the magnetic anomaly trends rotating from N-S to ENE-WSW. In both of these regions where fault strike azimuths are not subparallel to magnetic anomaly trends, fault lengths are generally shorter than in surrounding areas.

The dip of the incoming plate at the top of basement near the trench gradually increases from east to west, from a dip angle of ~1.6° seaward of the eastern portion of the Semidi segment between longitudes 156°W and 157°W, to 2.2° seaward of the westernmost part of the Shumagin Gap between longitudes 160°W and 161°W (Fig. 6). This increase in dip of the top of basement near the trench mirrors the dip at the seafloor in the outer rise (Fig. S-6) and the gradual increase in slab dip and curvature observed at greater depths (e.g., Fig. 1; Hayes et al., 2018; Kuehn, 2019).

Sediment thickness also varies along strike, with the thinnest sediment cover offshore of the Shumagin Gap (~400 m) in the western portion of the study area and the thickest sediment cover (~1100 m) offshore of the Semidi segment in the east (Fig. 4). The area of thin sediments east of the study area between ~152-148°W occurs in the area of the Patton Murray seamount chain (Fig. 4). We quantify the thickness of trench-fill sediments, as these sediments are deposited during bending and subduction and thus have the greatest potential to mask bending faulting at the seafloor. Pelagic sediments and terrigenous Zodiac fan sediments were deposited on the oceanic plate prior to bending and are thus expected to be offset by these younger bending faults. Although trench fill sediments are up to 1.5 km thick, they are generally confined to a narrow (~10-20 km) region near the trench, and bending faulting extends upwards of 50-70 km from the trench.

5 Discussion

5.1 Estimating bending fault throw and the impact of sediment cover on fault mapping

Cumulative bending-related fault throw is greatest outboard of the western Shumagin Gap between 159-161°W and decreases eastward from 158°W to 156°W; east of 156°W, no bending faulting is apparent in the bathymetry or seismic data (Figs. 2, 5, 7). Faults that may be evident in the igneous crust observed in seismic data east of ~156°W are most likely features created during crust formation. The crust in this region formed at slower spreading rates than crust to the west (Engebretson et al., 1985), creating a rougher crust surface (Buck et al., 2005; Buck & Poliakov, 1998; Carbotte & Macdonald, 1994). Possible faulting that may exist in the sediment cover offshore of the eastern Semidi segment (Fig 5B) is therefore not likely caused by active faulting and may instead be caused by differential compaction of sediments over a fractured crust surface

(Carvers, 1968). Here, all linear features observed in bathymetry data are oriented roughly N-S (Fig. 2) and are interpreted as relict abyssal-hill spreading faults. These results are consistent with previous seismic reflection imaging of bending faults in widely spaced seismic reflection profiles and with a documented westward increase in the frequency of outer rise earthquakes (Matulka et al., 2022; Shillington et al., 2015).

One possible contribution to the apparent eastward decrease in cumulative fault throw at the seafloor could be masking by sediments, which increases in thickness to the east (e.g., Shillington et al., 2015; Li et al., 2018, von Huene et al., 2012, Fig. 4). Sediment cover in the study area consists of three primary packages: pelagic sediments, terrigenous fan sediments, and Quaternary trench fill (Creager et al., 1973; Stevenson et al., 1983; von Huene et al., 2012). Our new sediment thickness grid shows an increase in total sediment thickness between $\sim 155^{\circ}\text{W}$ and 157°W as compared to the rest of the study area (Figs. 4, 7); this can be largely attributed to the presence of the Oligocene-Miocene aged terrestrial Zodiac fan, contributing >500 m of pelagic sediment and terrigenous turbidites (Creager et al., 1973; Stevenson et al., 1983; von Huene et al., 2012). This fan formed off the coast of the Pacific Northwest and was transported on the Pacific plate through its northward migration over the last 32-40 Ma (Stevenson et al., 1983). The Zodiac fan and other pelagic sediments on the oceanic crust are older than active bending faults in the present-day outer rise. Active faulting due to plate bending should, therefore, cut these older sediments, and fault scarps should still be evident on the seafloor even in the region covered by the fan.

We mapped the thickness and extent of trench fill. Trench fill sediments are deposited primarily by along-trench transport (von Huene et al., 2012). Although trench fill is up to 1.5 km thick, it is generally confined to a narrow region (<20 km) near the trench and discontinuous along-strike from limited reflection imaging (e.g., Figs. 4, 5). Thus, we consider it unlikely that the observed eastward decrease in bending faulting is due to sediment masking.

5.2 Controls on bending faulting strike orientations and throw

New constraints on bending faulting from this study offer the opportunity to examine controls on the orientations of bending faults and along-strike variations in cumulative outer rise fault throws.

5.2.1 Bending fault strike orientations

Previous analyses on controls on bending fault formation (e.g., Billen et al., 2007; Masson, 1991) found that abyssal-hill faults are reactivated when those abyssal-hill faults are oriented <25 - 30° of the trench and bending forms new faults when the angle between the spreading fabric and trench is >25 - 30° . Bending-related faults that reactivate pre-existing abyssal hill faults are expected to strike parallel to magnetic anomalies generated by seafloor spreading, and newly formed faults are expected to strike parallel the trench axis. In our study area, most bending faults strike parallel to magnetic anomalies suggesting that they formed by reactivation (Fig. 3), consistent with the previous studies of this area (Masson, 1991; Shillington et al., 2015). This is also consistent with observations at other subduction zones where pre-existing structures are near parallel to the trench, including the western Aleutians (Masson, 1991; Mortera-Gutiérrez et al.,

2003), offshore Nicaragua (Ranero et al., 2003; Van Avendonk et al., 2011), and in the Kuril subduction zone (Kobayashi et al., 1998, Fujie et al., 2018).

The average throws (~300 m) and average spacing (~3 km) of bending faults offshore of the Alaska Peninsula are similar to the characteristics of bending faults in other locations where bending occurs primarily by reactivation of abyssal hill faults (e.g., Ranero et al., 2003; Fujie et al., 2018). Fault spacing is ~5 km at the Kuril trench (Fujie et al., 2018) and ~2 km at the Middle America Trench (Faccenda et al., 2009; Ranero et al., 2003) where abyssal-hill faults are reactivated. When new bending faults form and cut across pre-existing fabrics, they often have larger throws and are more widely spaced compared to reactivated faults, as is observed at the Chilean and northern Japan trenches (e.g., Fujie et al., 2018; Geersen et al., 2018). In the eastern part of our study area ($<156^{\circ}\text{W}$), where pre-existing structures are oblique to the trench, bending faults are not observed (Fig. 8B). We discuss a possible explanation for the absence of bending faulting in the east in Section 5.2.2.

There are two regions within our study area ($156\text{-}157^{\circ}\text{W}$ and $159\text{-}160^{\circ}\text{W}$, Fig 3) that exhibit bending faults with a broader range of strikes that do not parallel magnetic anomalies. The region between $156\text{-}157^{\circ}\text{W}$ occurs north of the relict ridge-ridge-ridge triple junction and thus may have more complicated pre-existing structures. Complex and evolving abyssal-hill faulting is observed near modern ridge-ridge-ridge triple junctions and other areas of spreading changes (Smith et al., 2011), and the same may have been true in this area. We discuss the region between $159\text{-}160^{\circ}\text{W}$ in Section 5.3

5.2.2 Cumulative bending-related fault throw

We observe a significant westward increase in cumulative throw summed across all mapped faults (Fig. 7). Slab curvature is thought to be a primary control on the amount of slip on bending faults, where higher degrees of slab bending are expected to be associated with larger magnitudes of cumulative fault slip (Faccenda, 2014). In our study area, the bending angle of the incoming plate estimated from the dip of the top of basement crust in seismic reflection data (Fig. 6) steepens to the west, consistent with westward steepening of slab dip and increase in slab curvature at depth (Fig. 1; Buffett & Heuret, 2011; Hayes et al., 2018; Kuehn, 2019). This correlation suggests that the increase in slab dip could contribute the westward increase in cumulative bending faulting. However, given the relatively modest changes in slab curvature along-strike of $\sim 1^\circ$ over five degrees of longitude, it is surprising that we observe such a large and abrupt along-strike change in the amount of bending faulting: from no discernable bending faulting east of 156°W to significant bending faulting between $159\text{--}161^\circ\text{W}$. Therefore, while changes in slab dip likely contribute to the westward increase in observed cumulative bending faulting, other factors appear necessary to explain the relatively abrupt along-strike change in summed fault throws.

An abrupt change in pre-existing fabric in the subducting plate provides one possible explanation for the abrupt change in observed summed fault throws between $156\text{--}158^\circ\text{W}$. Magnetic anomaly patterns suggest that pre-existing structures west of 158°W are E-W striking and thus near parallel to the trench and favorable for reactivation, while east of 156°W they strike $\sim\text{N-S}$, up to 70° oblique to the trench (Fig. 2C; Shillington et al., 2015), unfavorable for reactivation. In the transition between these domains ($156\text{--}158^\circ\text{W}$), the near-trench magnetic anomalies generally

trend E-W, but they become weaker and less linear as one moves east, perhaps due to proximity to the relict triple junction directly to the south, and the transition to orthogonal (N-S) fossil ridge orientation directly to the east as discussed above (Fig. 2C, Engebretson et al., 1985; Lonsdale, 1988). Abundant faults are observed within this transition (Figure 3), but their cumulative slip is relatively modest (Figure 7), perhaps due to the complicated spreading fabric. In this scenario, reactivation of remnant structures, which are estimated to be ~30% weaker than the surrounding crust (Billen et al., 2007), allow extensional strain in the upper lithosphere to be accommodated by faulting west of ~158°W. In contrast, to the east, where favorably oriented weaknesses diminish and eventually disappear, bending stresses may not exceed the yield strength of the upper lithosphere and thus limited faulting occurs. This interpretation implies that bending stresses alone may be insufficient to promote the formation of outer rise faults in the oceanic lithosphere in locations that have modest slab dip and that lack inherited weaknesses. For comparison, slab dip is significantly steeper (by ~2°) in other subduction zones where new bending faults form without reactivating pre-existing structures (e.g., Kurile and Chilean subduction zones; (Fujie et al., 2013; Nishikawa & Ide, 2015; Ranero et al., 2005).

It has been hypothesized that weakening of the oceanic plate by faulting at the outer rise and associated hydration and serpentinization could provide a positive feedback to induce additional slab bending and outer rise faulting (Billen & Gurnis, 2005; Contreras-Reyes & Osses, 2010; Faccenda et al., 2012; Hyndman & Peacock, 2003; Ranero et al., 2003). In Alaska, favorably oriented pre-existing structures may be important for this feedback to initiate as they allow faulting and hydration even at modest bending angles. The long wavelength over which slab dip steepens along the Alaska subduction zone primarily reflects the transition from flat-slab

subduction in the Gulf of Alaska to the east (Davis & Plafker, 1986; Petersen et al., 2021) to normal ocean-ocean plate subduction to the west. The rapid transition in bending-related faulting observed in our region may induce an additional short-wavelength transition in plate weakening that may enhance westward slab steepening. A westward reduction in plate strength at the outer-trench slope is also consistent with a decrease in the distance from the trench where bending faulting initiates: up to ~75 km from trench at ~157°W but confined to <50 km from trench farther west (Fig. 2). Bending and faulting are expected to occur over larger wavelengths for stronger plates. Similar relationships between pre-existing structures, outer rise faulting, and slab bending angles are observed in the Middle America subduction zone offshore Costa Rica and Nicaragua (Ranero et al., 2003).

In summary, we propose that the combination of along-strike changes in slab dip and the orientation of pre-existing structures with respect to the trench best explains a relatively abrupt along-strike change in the amount of faulting. The steeper slab dips and favorably oriented pre-existing structures, which are weaker than the surrounding crust, allow bending faulting in the west. In the east, bending stresses associated with modest slab bending may not exceed the yield strength of the lithosphere, and pre-existing structures are highly oblique to the trench, so limited faulting is observed. Feedbacks between pre-existing structures, bending faulting, and plate weakening may further promote faulting in the west (e.g., Billen & Gurnis, 2005; Contreras-Reyes & Osses, 2010).

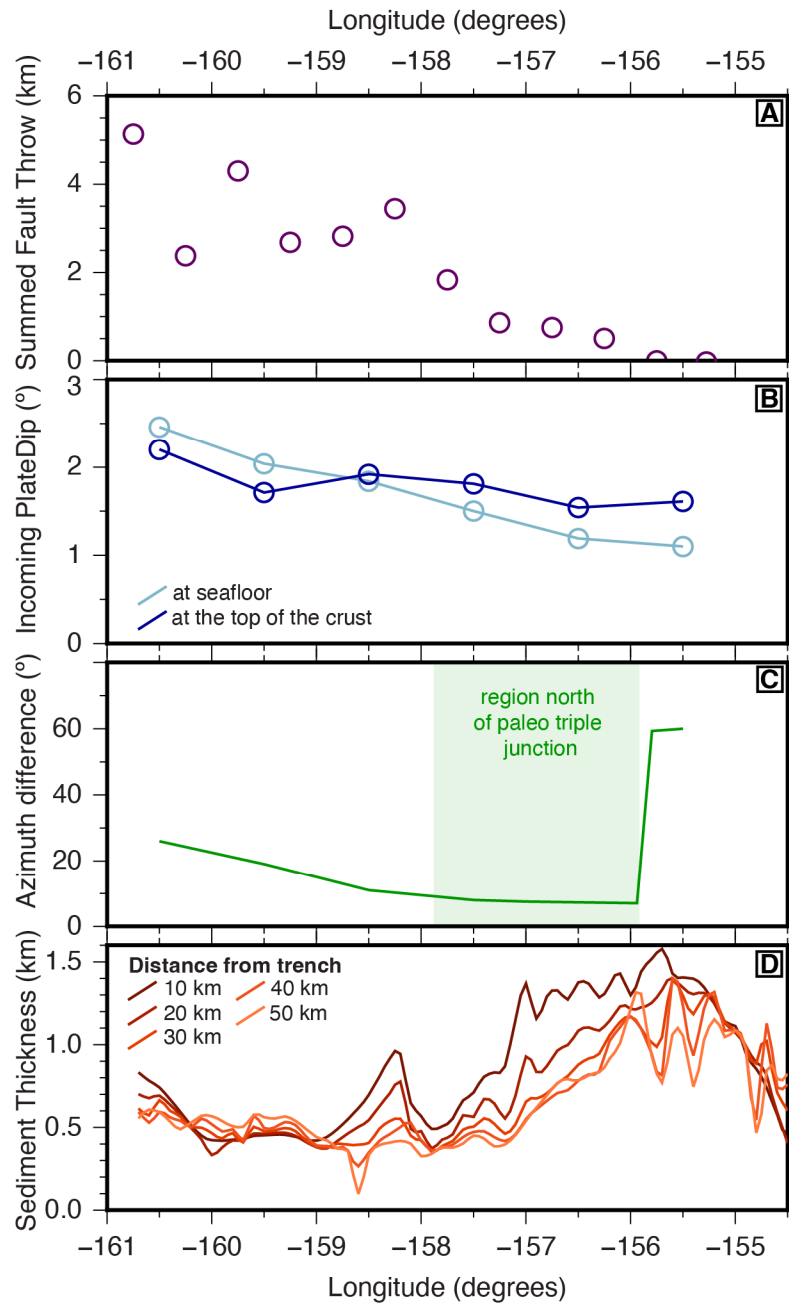


Figure 7: Along strike variations in a) summed maximum throws on bending faults within 0.5°-wide bins; b) dip of the subducting plate at the outer rise, estimated from bathymetric seafloor slope (light blue, Fig. S6) and from the dip of the top of the crust based on a structure contour map of the base of incoming plate sediments (dark blue, Fig. 6); c) difference between the expected strike of pre-existing structures from magnetic anomalies and the trench; d) incoming plate sediment thickness on the incoming plate at distances of 10-50 km from the trench.

5.3 Complex faulting and possible linkage to October 2022 M7.6 intraplate event

Between $\sim 159\text{-}160^\circ\text{W}$, we observe an area of relatively complex bending-related faulting (Figs. 3, 9). Outside of this area, fault orientations generally exhibit a single, dominant peak in azimuth centered around the average trend of magnetic anomalies ($\sim 85\text{-}90^\circ$). Within the complex zone, a peak is still observed at $\sim 85^\circ$, but with an additional broad plateau with abundant faulting spanning orientations between $35\text{-}80^\circ$ (Fig. 3). At $\sim 159.25^\circ\text{W}$, we also observe a series of features that we interpret as small volcanic constructs (Fig. 8). Similar features are recognized in the outer rises of other subduction zones (e.g., Japan trench; Fujie et al., 2020; Hirano, 2011; Hirano et al., 2006) and categorized as petit-spot magmatism. Off Japan, petit-spot volcanic provinces do not geochemically resemble mid-ocean ridge melts or occur near hotspot centers and are thus hypothesized to be caused by partial melting of the asthenosphere induced by plate bending and fracturing (Hirano et al., 2006).

The complex faulting in this region suggests comparable complexity in the pre-existing structures or stress state of the incoming plate in this region. Magnetic anomalies are relatively continuous through this region, and thus there is no evidence for the former here. Given the short length scales associated with the complexity, we require a mechanism that can produce a relatively abrupt changes in plate stress. Geodetic observations indicate a relatively abrupt change in megathrust coupling between the Shumagin Gap ($\sim 159\text{-}162^\circ\text{W}$) and the Semidi segment ($\sim 155\text{-}159^\circ\text{W}$; Drooff & Freymueller, 2021; Xiao et al., 2021), with a transition approximately coincident with the region of complex faulting. Along-strike variations in megathrust coupling and coseismic slip have been invoked to explain differences in incoming plate seismicity in many subduction zones (e.g., Christensen & Ruff, 1988; Emry et al., 2014),

and it is possible that changes in coupling could also cause complexities in stress in the incoming plate over long time periods and thus explain the complex bending-related faulting we observe. Complex patterns of stress and faulting within the incoming plate could also promote the generation of small amount of melt and intraplate volcanism.

The region of complex faulting and petit-spot volcanism that we observe between 159-160°W lies directly updip from the Oct 2020 M7.6 intraplate event raising the possibility that they could have related origins. Two causes have been proposed for this enigmatic earthquake, which appears to have ruptured a steep fault in the subducting plate that strikes ~15° and thus orthogonal to the trench: 1) reactivation of remnant spreading features produced at the Kula-Resurrection ridge, which is now subducted (Fuston & Wu, 2020; Jiang et al., 2022); 2) accumulated shear stresses caused by lateral variability in slab dip and coupling (Herman & Furlong, 2021). In the first case, the 2020 M7.6 event is modeled as right-lateral strike-slip motion on a N-S striking fault dipping steeply to the east (Jiang et al., 2020), with slip distribution and associated aftershocks extending to within 30 km laterally from the zone of complex faulting. If this event reactivates hypothesized pre-existing Kula-Resurrection fabric just north of the trench (Fuston and Wu, 2020), then it is plausible that persistent slip on this feature has induced static stress changes in the incoming plate just up-dip of the fault tip (Yang et al., 2023) that are sufficient to perturb the bending stresses and associated fault orientations. In the second case, accumulated stresses in the subducting plate arising from lateral variability in coupling between the Shumagin Gap and Semidi segment could explain both the occurrence of the M7.6 intraplate earthquake (Herman & Furlong, 2021) and the complexities we observe bending-related faulting patterns outboard of the trench. Although more work is needed to

evaluate the influence of changes in megathrust coupling on long-term deformation in the incoming plate, the spatial proximity of the earthquake and complex faulting imply a common origin.

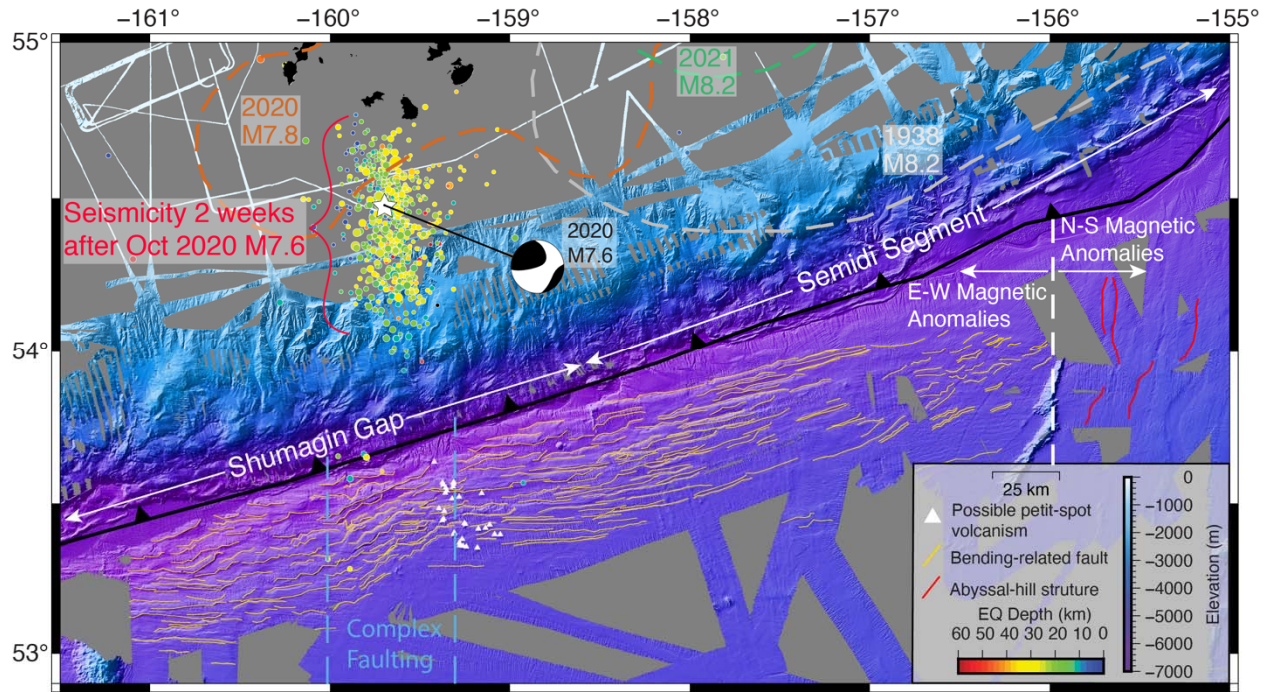


Figure 8: Bathymetric map of bending-related faulting (yellow lines) with abyssal-hill structures (red lines). Also shown is the CMT solution (Dziwonski et al., 1981; Ekström et al., 2012) for the Oct 2020 M7.6 intraplate event and earthquakes two weeks after the M7.6 (points colored by depth; from the Alaska Earthquake Information Center). Highlighted between the dashed blue lines is an area of complex bending faulting between ~159.25-160°W, which lies immediately updip of the 2020 M7.6 intraplate event. Interpreted petit-spot volcanism (white triangles) at ~159.25°W occurs on the eastern edge of the region of complex faulting. Large megathrust rupture patches are shown on the overriding plate colored the same as previous figures.

5.4 Implications for hydration

One major importance of bending-related faulting is its role in allowing ingress of seawater and hydration of the crust and upper mantle of the incoming plate (Cai et al., 2018; Faccenda, 2014; Faccenda et al., 2009; Grevemeyer et al., 2018; Ivandic et al., 2008; Korenaga, 2017; Nishikawa

& Ide, 2015; Peacock, 2001; Ranero et al., 2003; Shillington et al., 2015). Extensional faults on the incoming plate are thought to act as conduits for seawater to percolate several kilometers through the crust and into the upper mantle of the incoming plate. The water may reside as fluid-filled cracks in the crust and upper mantle (Miller et al., 2021), as well as react with the ultramafic peridotites and form serpentinite (Carlson & Miller, 2003; Faccenda, 2014; Faccenda et al., 2009; Grevemeyer et al., 2018; Korenaga, 2017; Peacock, 2001; Ranero et al., 2003). Seismic velocity models from subduction zones around the globe show the reduced velocities in the crust and upper mantle of the subducting plate near the trench, which are interpreted to represent the presence of hydrous minerals and or fluid-filled cracks (Cai et al., 2018; Contreras-Reyes et al., 2007, 2011; Fujie et al., 2018; Ivandic et al., 2008; Shillington et al., 2015; Van Avendonk et al., 2011).

P-wave velocity models in the study area exhibit a more pronounced reduction in seismic velocity in the upper mantle of the incoming plate outboard of the Shumagin Gap (western portion of the study area; west of $\sim 157^{\circ}\text{W}$) than in the Semidi segment (eastern portion of the study area; east of $\sim 157^{\circ}\text{W}$), suggesting greater hydration in the west (Shillington et al., 2015). Likewise, high-resolution P-wave models from streamer tomography also show a reduction in velocity in the upper crust, interpreted to arise from a combination of faulting and alteration (Acquisto et al., 2022). The combination of preferentially oriented pre-existing structures and an increase in slab dip outboard of the Shumagin Gap promote more bending faulting and are thus expected to produce increasing hydration of the incoming lithosphere. A westward increase in hydration can be inferred from the westward increase in number of faults and larger fault throws and is consistent with observations of a double-seismic zone in the downgoing plate in the

Shumagin Gap, prominent conductors at depth in magnetotelluric data (Cordell et al., 2023), and geochemical signatures consistent with fluids in arc volcanism in the western Shumagin Gap (Wei et al., 2021).

5.5 Implications for plate boundary properties

Westward increases in the total number and throws of bending-related faults on the incoming plate, combined with decreasing westward sediment thickness, can influence the heterogeneity of the megathrust interface once subducted. For example, rough seafloor is proposed to promote creeping of the megathrust interface and numerous small to medium ($< M7.5$) events (Wang & Bilek, 2014) and potentially contribute to slow slip events (e.g., Saffer & Wallace, 2015). Higher degrees of bending faulting to the west are also expected to result in greater hydration of the crust and upper mantle, stored in hydrous minerals or as free water. Dehydration and migration of fluids at depth could also influence megathrust properties and behavior (e.g., Cordell et al., 2023; Saffer & Tobin, 2011; Saffer & Wallace, 2015). Increased total faulting and larger faults to the west, with a thinner sediment cover, allowing for greater degree of hydration of the incoming plate, may lead to a heterogeneous megathrust interface and promote creep.

Geodetic studies of the Alaska Peninsula show that the western Shumagin Gap, which has increased bending faulting, crustal and upper mantle hydration, and thinner sediments, is $< 30\%$ coupled, whereas the eastern Semidi segment is almost entirely locked (Drooff & Freymueller, 2021; Li & Freymueller, 2018). The lack of bending faulting and larger amounts of sediment entering the subduction zone in the eastern Semidi segment (Li et al., 2018) could contribute to greater megathrust homogeneity, allowing for locking along the interface and increasing the

potential for great earthquakes in the eastern portion of our study area. Our results show that the western part of the study area outboard of the Shumagin Gap has increased fault throws creating a highly fractured plate with low sediment cover. These conditions likely lead to a heterogeneous, fluid rich plate interface which may promote creep in the Shumagin Gap region (Bécel et al., 2017; Cordell et al., 2023).

6 Conclusions

Analysis of new high-resolution bathymetry data collected outboard of the Shumagin Gap and Semidi segment provide new insights into controls on formation and patterns of bending-related faulting in the outer-rise of the incoming Pacific plate.

1) Bending-related faults strike dominantly parallel to magnetic anomalies, indicating that bending primarily reactivates relict abyssal-hill faults originating at oceanic plate formation. The angle between magnetic anomalies and the trench controls bending fault strike, where reactivated faults parallel magnetic anomalies and newly formed faults parallel the trench.

2) The plate bends more steeply to the west in the Shumagin Gap region, where observed faulting is more extensive and where larger faults, with greater throw, form. These observations suggest that increased bending of the downgoing plate is likely one contributing factor to the westward increase in summed scarp heights. However, feedbacks between pre-existing structures, slab weakening, and bending and faulting appear necessary to explain the relatively abrupt along-strike changes in the amount of bend faulting.

3) The subducting plate updip of the M7.6 intraplate earthquake (between 159-160°W) exhibits relatively complex bending faulting and petit spot volcanism. Variations in coupling and slab dip could contribute to both bending faulting patterns and the M7.6 earthquake here.

4) The westward increase in bending faulting has important implications for incoming plate weaknesses and the ability for bending-faulting to pervasively hydrate the incoming plate at the western Shumagin Gap.

5) Thin sediment cover and pervasive bending-related faulting on the incoming plate outboard of the western Shumagin Gap promotes a heterogeneous, fluid rich plate interface and creeping megathrust behavior at depth. Thick sediment cover and nearly absent bending-related faulting on the incoming plate outboard of the eastern Semidi segment promotes a homogeneous megathrust, contributing to recurring great earthquakes.

Acknowledgements

We gratefully acknowledge the scientists and ship crews of the R/V *Langseth* and R/V *Sikuliaq* responsible for the collection of bathymetry data during the Alaska Amphibious Community Seismic Experiment (AACSE). This work was supported by NSF-OCE-2026676 to NAU and NSF-OCE- 2025969 to Washington University. Freely available Generic Mapping Tools (GMT) and OpendTect software were used in data analysis and display.

Open Research

All of the data used in this paper are opening available. Bathymetry data can be accessed through the Marine Geoscience Data System (<https://www.marine-geo.org/index.php>). Seismic reflection data from ALEUT (<https://www.marine-geo.org/tools/entry/MGL1110>) and AACSE (<https://www.marine-geo.org/tools/entry/MGL1903>) are also available through the MGDS.

References

- Abers, G. A. (1992). Relationship between shallow-and-intermediate depth seismicity in the eastern Aleutian subduction zone. *Physics of the Earth and Planetary Interiors*, 19, 2019–2022. <http://linkinghub.elsevier.com/retrieve/pii/S0031920104001657>
- Acquisto, T., Bécel, A., Singh, S. C., & Carton, H. (2022). Evidence of strong upper oceanic crustal hydration outboard the Alaskan and Sumatran subduction zones. *Journal of Geophysical Research: Solid Earth*, 127, e2022JB024751.
- Bankey, V., Cuevas, A., Daniels, D. L., Finn, C. A., Hernandez, I., Hill, P. L., Kucks, R., Miles, W., Pilkington, M., Roberts, C., Roest, W., Rystrom, V., Shearer, S., Snyder, S. L., Sweeney, R. E., & Velez, J. (2002). *Magnetic anomaly map of North America*. <https://doi.org/10.3133/70211067>
- Barcheck, G., Abers, G. A., Adams, A. N., Bécel, A., Collins, J., Gaherty, J. B., Haeussler, P. J., Li, Z., Moore, G., Onyango, E., Roland, E., Sampson, D. E., Schwartz, S. Y., Sheehan, A. F., Shillington, D. J., Shore, P. J., Webb, S., Wiens, D. A., & Worthington, L. L. (2020). The Alaska Amphibious Community Seismic Experiment. *Seismological Research Letters*, 91(6), 3054–3063. <https://doi.org/10.1785/0220200189>
- Bécel, A., Sheehan, A., Foster, D., Myers, E., Haeussler, P., Abers, G., Adams, A., Roland, E., Schwartz, S., Shillington, D., Wiens, D., Webb, S., & L. Worthington. (2019). Multi-Channel Seismic Shot Data from the Alaska-Aleutians area acquired during Langseth cruise MGL1903. In *IEDA*. <https://doi.org/10.1594/IEDA/324793>
- Bécel, A., Shillington, D. J., Delescluse, M., Nedimović, M. R., Abers, G. A., Saffer, D. M., Webb, S. C., Keranen, K. M., Roche, P. H., Li, J., & Kuehn, H. (2017). Tsunamigenic

structures in a creeping section of the Alaska subduction zone. *Nature Geoscience*,
 10(8), 609–613. <https://doi.org/10.1038/NGEO2990>

Bécel, A., Shillington, D. J., Nedimović, M. R., Webb, S. C., & Kuehn, H. (2015). Origin of
 dipping structures in fast-spreading oceanic lower crust offshore Alaska imaged by
 multichannel seismic data. *Earth and Planetary Science Letters*, 424, 26–37.
<https://doi.org/10.1016/j.epsl.2015.05.016>

Billen, M. I., & Gurnis, M. (2005). Constraints on subducting plate strength within the
 Kermadec trench. *Journal of Geophysical Research: Solid Earth*, 110(5), 1–18.
<https://doi.org/10.1029/2004JB003308>

Bodine, J. H., & Watts, A. B. (1979). On lithospheric flexure seaward of the Bonin and
 Mariana trenches. *Earth and Planetary Science Letters*, 43, 132–148.

Boneh, Y., Schottenfels, E., Kwong, K., van Zelst, I., Tong, X., Eimer, M., Miller, M. S.,
 Moresi, L., Warren, J. M., Wiens, D. A., Billen, M., Naliboff, J., & Zhan, Z. (2019).
 Intermediate-Depth Earthquakes Controlled by Incoming Plate Hydration Along
 Bending-Related Faults. *Geophysical Research Letters*, 46(7), 3688–3697.
<https://doi.org/10.1029/2018GL081585>

Buck, W. R., Lavier, L. L., & Poliakov, A. N. B. (2005). Modes of faulting at mid-ocean
 ridges. *Nature*, 434(7034), 719–723. <https://doi.org/10.1038/nature03358>

Buck, W. R., & Poliakov, A. N. B. (1998). Abyssal hills formed by stretching oceanic
 lithosphere. *Nature*, 392, 272–275. <https://doi.org/10.1038/246170a0>

Buffett, B. A., & Heuret, A. (2011). Curvature of subducted lithosphere from earthquake
 locations in the Wadati-Benioff zone. *Geochemistry, Geophysics, Geosystems*, 12(6),
 Q06010. <https://doi.org/10.1029/2011GC003570>

- Buurman, H., Nye, C. J., West, M. E., & Cameron, C. (2014). Regional controls on volcano seismicity along the Aleutian arc. *Geochemistry, Geophysics, Geosystems*, 15, 1147–1163. <https://doi.org/10.1002/2013GC005101>
- Cai, C., Wiens, D. A., Shen, W., & Eimer, M. (2018). Water input into the Mariana subduction zone estimated from ocean-bottom seismic data. *Nature*, 563, 389–392. <https://doi.org/10.1038/s41586-018-0655-4>
- Caldwell, J. G., Haxby, W. F., Karig, D. E., & Turcotte, D. L. (1976). On the applicability of a universal elastic trench profile. *Earth and Planetary Science Letters*, 31, 239–246.
- Canales, J. P., Carbotte, S. M., Nedimovic, M. R., & Carton, H. (2017). Dry Juan de Fuca slab revealed by quantification of water entering Cascadia subduction zone. *Nature Geoscience*, 10(11), 864–870. <https://doi.org/10.1038/NGEO3050>
- Carbotte, S. M., & Macdonald, K. C. (1994). Comparison of seafloor tectonic fabric at intermediate, fast, and super fast spreading ridges: Influence of spreading rate, plate motions, and ridge segmentation on fault patterns. *Journal of Geophysical Research*, 99(B7), 13609–13631. <https://doi.org/doi:10.1029/93JB02971>
- Carlson, R. L., & Miller, D. J. (2003). Mantle wedge water contents estimated from seismic velocities in partially serpentinized peridotites. *Geophysical Research Letters*, 30(5), 12–15. <https://doi.org/10.1029/2002gl016600>
- Carvers, R. E. (1968). Differential Compaction as a Cause of Regional Contemporaneous Fault. *American Association of Petroleum Geologists Bulletin*, 52(3), 414–419. http://pubs.geoscienceworld.org/aapgbull/article-pdf/52/3/414/4456253/aapg_1968_0052_0003_0414.pdf

- Chapple, W. M., & Forsyth, D. W. (1979). Earthquakes and Bending of Plates at Trenches. *Journal of Geophysical Research*, 84(B12), 6729–6749.
- Christensen, D. H., & Ruff, L. J. (1988). Seismic Coupling and Outer Rise Earthquakes. *Journal of Geophysical Research*, 93(B11), 13,421–13,444.
<https://doi.org/10.1029/JB093iB11p13421>
- Contreras-Reyes, E., Grevemeyer, I., Flueh, E. R., Scherwath, M., & Bialas, J. (2008). Effect of trench-outer rise bending-related faulting on seismic Poisson's ratio and mantle anisotropy: A case study offshore of Southern Central Chile. *Geophysical Journal International*, 173, 142–156. <https://doi.org/10.1111/j.1365-246X.2008.03716.x>
- Contreras-Reyes, E., Grevemeyer, I., Flueh, E. R., Scherwath, M., & Heesemann, M. (2007). Alteration of the subducting oceanic lithosphere at the southern central Chile trench-outer rise. *Geochemistry, Geophysics, Geosystems*, 8(7), Q07003.
<https://doi.org/10.1029/2007GC001632>
- Contreras-Reyes, E., Grevemeyer, I., Watts, A. B., Flueh, E. R., Peirce, C., Moeller, S., & Papenberg, C. (2011). Deep seismic structure of the Tonga subduction zone: Implications for mantle hydration, tectonic erosion, and arc magmatism. *Journal of Geophysical Research*, 116(10), B10103. <https://doi.org/10.1029/2011JB008434>
- Contreras-Reyes, E., & Osses, A. (2010). Lithospheric flexure modelling seaward of the Chile trench: Implications for oceanic plate weakening in the Trench Outer Rise region. *Geophysical Journal International*, 182, 97–112.
<https://doi.org/10.1111/j.1365-246X.2010.04629.x>

- Cordell, D., Naif, S., Evans, R., Key, K., Constable, S., Shillington, D., & B  cel, A. (2023). Forearc seismogenesis in a weakly coupled subduction zone influenced by slab mantle fluids. *Nature Geoscience*, 16, 826827. <https://doi.org/10.1038/s41561-023-01260-w>
- Creager, J. S., Scholl, D. W., Boyce, R. E., Echols, R. J., Lee, H. J., Ling, H. Y., Stewart, R. J., Supko, P. R., & Worsley, T. R. (1973). Deep sea drilling project initial reports: site 183. *DSDP*, 19, 1–19.
- Davies, J., Sykes, L., House, L., & Jacob, K. (1981). Shumagin Seismic Gap, Alaska Peninsula: History of Great Earthquakes, Tectonic Setting, and Evidence for High Seismic Potential. *Journal of Geophysical Research*, 86(B5), 3821–3855. <https://doi.org/10.1029/JB086iB05p03821>
- Davis, A. S., & Plafker, G. (1986). Eocene basalts from the Yakutat terrane: Evidence for the origin of an accreting terrane in southern Alaska. *Geology*, 14, 963–966.
- Drooff, C., & Freymueller, J. T. (2021). New Constraints on Slip Deficit on the Aleutian Megathrust and Inflation at Mt. Veniaminof, Alaska From Repeat GPS Measurements. *Geophysical Research Letters*, 48, e2020GL091787. <https://doi.org/10.1029/2020GL091787>
- Dziewonski, A. M., Chou, T. A., & Woodhouse, J. H. (1981). Determination of earthquake source parameters from waveform data for studies of global and regional seismicity. *Journal of Geophysical Research*, 86(B4), 2825–2852. <https://doi.org/10.1029/JB086iB04p02825>
- Eimer, M., Wiens, D. A., Cai, C., Lizarralde, D., & Jaspersen, H. (2020). Seismicity of the Incoming Plate and Forearc Near the Mariana Trench Recorded by Ocean Bottom

- Seismographs. *Geochemistry, Geophysics, Geosystems*, 21(4).
<https://doi.org/10.1029/2020GC008953>
- Ekström, G., Nettles, M., & Dziewoński, A. M. (2012). The global CMT project 2004–2010: Centroid-moment tensors for 13,017 earthquakes. *Physics of the Earth and Planetary Interiors*, 200–201, 1–9.
<https://doi.org/https://doi.org/10.1016/j.pepi.2012.04.002>
- Elliot, J. L., Grapenthin, R., Parameswaran, R. M., Xiao, Z., Freymueller, J. T., & Fusso, L. (2022). Cascading rupture of a megathrust. *Science Advances*, 8, eabm4131.
- Emry, E. L., Wiens, D. A., & Garcia-Castellanos, D. (2014). Faulting within the Pacific plate at the Mariana Trench: Implications for plate interface coupling and subduction of hydrous minerals. *Journal of Geophysical Research, Solid Earth*, 119, 3076–3095.
<https://doi.org/10.1002/2013JB010718>
- Engelbreton, D. C., Cox, A., & Gordon, R. G. (1985). Relative Motions Between Oceanic Plates of the Pacific Basin. *Geological Society of America Special Paper*, 206, 1–60.
<https://doi.org/10.1029/JB089iB12p10291>
- Faccenda, M. (2014). Water in the slab: A trilogy. *Tectonophysics*, 614, 1–30.
<https://doi.org/10.1016/j.tecto.2013.12.020>
- Faccenda, M., Gerya, T. V., & Burlini, L. (2009). Deep slab hydration induced by bending-related variations in tectonic pressure. *Nature Geoscience*, 2, 790–793.
<https://doi.org/10.1038/ngeo656>
- Faccenda, M., Gerya, T. V., Mancktelow, N. S., & Moresi, L. (2012). Fluid flow during slab unbending and dehydration: Implications for intermediate-depth seismicity, slab

weakening and deep water recycling. *Geochemistry, Geophysics, Geosystems*, 13,
 Q01010. <https://doi.org/10.1029/2011GC003860>

Florez, M. A., & Prieto, G. A. (2019). Controlling Factors of Seismicity and Geometry in
 Double Seismic Zones. *Geophysical Research Letters*, 46(8), 4174–4181.
<https://doi.org/10.1029/2018GL081168>

Fujie, G., Kodaira, S., Kaiho, Y., Yamamoto, Y., Takahashi, T., Miura, S., & Yamada, T.
 (2018). Controlling factor of incoming plate hydration at the north-western Pacific
 margin. *Nature Communications*, 9. <https://doi.org/10.1038/s41467-018-06320-z>

Fujie, G., Kodaira, S., Nakamura, Y., Morgan, J. P., Dannowski, A., Thorwart, M.,
 Grevenmeyer, I., & Miura, S. (2020). Spatial variations of incoming sediments at the
 northeastern Japan arc and their implications for megathrust earthquakes. *Geology*,
 48(6), 614–619. <https://doi.org/10.1130/G46757.1>

Fujie, G., Kodaira, S., Yamashita, M., Sato, T., Takahashi, T., & Takahashi, N. (2013).
 Systematic changes in the incoming plate structure at the Kuril trench. *Geophysical
 Research Letters*, 40(1), 88–93. <https://doi.org/10.1029/2012GL054340>

Fuston, S., & Wu, J. (2020). Raising the Resurrection plate from an unfolded-slab plate
 tectonic reconstruction of northwestern North America since early Cenozoic time.
Bulletin of the Geological Society of America, 133(5), 1128–1140.
<https://doi.org/10.1130/B35677.1>

Garcia, E. S. M., Sandwell, D. T., & Bassett, D. (2019). Outer trench slope flexure and
 faulting at Pacific basin subduction zones. *Geophysical Journal International*, 218,
 708–728. <https://doi.org/10.1093/gji/ggz155>

- Geersen, J., Ranero, C. R., Klaucke, I., Behrmann, J. H., Kopp, H., Tréhu, A. M., Contreras-Reyes, E., Barckhausen, U., & Reichert, C. (2018). Active Tectonics of the North Chilean Marine Forearc and Adjacent Oceanic Nazca Plate. *Tectonics*, 37(11), 4194–4211. <https://doi.org/10.1029/2018TC005087>
- Grevenmeyer, I., Ranero, C. R., & Ivandic, M. (2018). Structure of oceanic crust and serpentinization at subduction trenches. *Geosphere*, 14(2), 395–418. <https://doi.org/10.1130/GES01537.1>
- Hacker, B. R. (2008). H₂O subduction beyond arcs. *Geochemistry, Geophysics, Geosystems*, 9(3), Q03001. <https://doi.org/10.1029/2007GC001707>
- Hasegawa, A., & Nakajima, J. (2017). Seismic imaging of slab metamorphism and genesis of intermediate-depth intraslab earthquakes. *Progress in Earth and Planetary Science*, 4. <https://doi.org/10.1186/s40645-017-0126-9>
- Hayes, G. P., Moore, G. L., Portner, D. E., Hearne, M., Flamme, H., Furtney, M., & Smoczyk, G. M. (2018). Slab2, a comprehensive subduction zone geometry model. *Science*, 362(6410), 58–61. <https://doi.org/10.1126/science.aat4723>
- Herman, M. W., & Furlong, K. P. (2021). Triggering an unexpected earthquake in an uncoupled subduction zone. *Science Advances*, 7(13), eabf7590. <https://doi.org/10.1126/sciadv.abf7590>
- Hilde, T. W. C. (1983). Sediment subduction versus accretion around the pacific. *Tectonophysics*, 99, 381–397. [https://doi.org/10.1016/0040-1951\(83\)90114-2](https://doi.org/10.1016/0040-1951(83)90114-2)
- Hirano, N. (2011). Petit-spot volcanism: A new type of volcanic zone discovered near a trench. *Geochemical Journal*, 45, 157–167. <https://doi.org/10.2343/geochemj.1.0111>

- Hirano, N., Takahashi, E., Yamamoto, J., Abe, W., Ingle, S. P., Kaneoka, I., Hirata, T., Kimura, J. I., Ishii, T., Ogawa, Y., Machida, S., & Suyehiro, K. (2006). Volcanism in response to plate flexure. *Science*, 313, 1426–1428.
<https://doi.org/10.1126/science.1128235>
- Holt, A. F., Buffett, B. A., & Becker, T. W. (2015). Overriding plate thickness control on subducting plate curvature. *Geophysical Research Letters*, 42(10), 3802–3810.
<https://doi.org/10.1002/2015GL063834>
- Hyndman, R. D., & Peacock, S. M. (2003). Serpentinization of the forearc mantle. *Earth and Planetary Science Letters*, 212, 417–432. [https://doi.org/10.1016/S0012-821X\(03\)00263-2](https://doi.org/10.1016/S0012-821X(03)00263-2)
- Ivandic, M., Grevemeyer, I., Berhorst, A., Flueh, E. R., & McIntosh, K. (2008). Impact of bending related faulting on the seismic properties of the incoming oceanic plate offshore of Nicaragua. *Journal of Geophysical Research*, 113, B05410.
<https://doi.org/10.1029/2007JB005291>
- Iyer, K., Rüpke, L. H., Morgan, J. P., & Grevemeyer, I. (2012). Controls of faulting and reaction kinetics on serpentinization and double Benioff zones. *Geochemistry, Geophysics, Geosystems*, 13(9), Q09010. <https://doi.org/10.1029/2012GC004304>
- Jiang, Y., González, P. J., & Bürgmann, R. (2022). Subduction earthquakes controlled by incoming plate geometry: The 2020 $M > 7.5$ Shumagin, Alaska, earthquake doublet. *Earth and Planetary Science Letters*, 584, 117447.
<https://doi.org/10.1016/j.epsl.2022.117447>
- Kita, S., Okada, T., Nakajima, J., Matsuzawa, T., & Hasegawa, A. (2006). Existence of a seismic belt in the upper plane of the double seismic zone extending in the along-arc

direction at depths of 70-100 km beneath NE Japan. *Geophysical Research Letters*, 33(24), L24310. <https://doi.org/10.1029/2006GL028239>

Kobayashi, K., Nakanishi, M., Tamaki, K., & Ogawa, Y. (1998). Outer slope faulting associated with the western Kuril and Japan trenches. *Geophysical Journal International*, 134(2), 356–372. <https://doi.org/10.1046/j.1365-246X.1998.00569.x>

Kobayashi, K., Tamaki, K., Nakanishi, M., Korenaga, J., & Ogawa, Y. (1995). Rejuvenation of 130 m.y.-old Fabrics on the Outer Wall of the Western Kuril Trench. *Proceedings of the Japan Academy*, 71(B), 5–9.

Korenaga, J. (2017). On the extent of mantle hydration caused by plate bending. *Earth and Planetary Science Letters*, 457, 1–9. <https://doi.org/10.1016/j.epsl.2016.10.011>

Kuehn, H. (2019). *Along-trench segmentation and down-dip limit of the seismogenic zone at the eastern Alaska-Aleutian subduction zone* [PhD]. Dalhousie University, Halifax, Nova Scotia.

Lay, T., Ammon, C. J., Kanamori, H., Kim, M. J., & Xue, L. (2011). Outer trench-slope faulting and the 2011 Mw 9.0 off the Pacific coast of Tohoku Earthquake. *Earth, Planets and Space*, 63(37), 713–718. <https://doi.org/10.5047/eps.2011.05.006>

Lay, T., Kanamori, H., Ammon, C. J., Hutko, A. R., Furlong, K., & Rivera, L. (2009). The 2006-2007 Kuril Islands great earthquake sequence. *Journal of Geophysical Research*, 114, B11308. <https://doi.org/10.1029/2008JB006280>

Lefeldt, M., Ranero, C. R., & Grevemeyer, I. (2012). Seismic evidence of tectonic control on the depth of water influx into incoming oceanic plates at subduction trenches. *Geochemistry, Geophysics, Geosystems*, 13(5), Q05013. <https://doi.org/10.1029/2012GC004043>

- Li, J., Shillington, D. J., Bécel, A., Nedimović, M. R., Webb, S. C., Saffer, D. M., Keranen, K. M., & Kuehn, H. (2015). Dondip variations in seismic reflection character: Implications for fault structure and seismogenic behavior in the Alaska subduction zone. *Journal of Geophysical Research: Solid Earth*, 120, 7883–7904.
<https://doi.org/10.1002/2015JB012338>
- Li, J., Shillington, D. J., Saffer, D. M., Bécel, A., Nedimović, M. R., Kuehn, H., Webb, S. C., Keranen, K. M., & Abers, G. A. (2018). Connections between subducted sediment, pore-fluid pressure, and earthquake behavior along the Alaska megathrust. *Geology*, 46(4), 299–302. <https://doi.org/10.1130/G39557.1>
- Li, S., & Freymueller, J. T. (2018). Spatial Variation of Slip Behavior Beneath the Alaska Peninsula Along Alaska-Aleutian Subduction Zone. *Geophysical Research Letters*, 45, 3453–3460. <https://doi.org/10.1002/2017GL076761>
- Liu, C., Lay, T., & Xiong, X. (2022). The 29 July 2021 M W 8.2 Chignik, Alaska Peninsula Earthquake Rupture Inferred From Seismic and Geodetic Observations: Re-Rupture of the Western 2/3 of the 1938 Rupture Zone. *Geophysical Research Letters*, 49, e2021GL096004. <https://doi.org/10.1029/2021gl096004>
- Lonsdale, P. (1988). Paleogene history of the Kula plate,: Offshore evidence and onshore implication. *Geological Society of America Bulletin*, 100, 733–754.
[https://doi.org/10.1130/0016-7606\(1988\)100<0733:PHOTKP>2.3.CO;2](https://doi.org/10.1130/0016-7606(1988)100<0733:PHOTKP>2.3.CO;2)
- Macdonald, K. C., Fox, P. J., Alexander, R. T., Pockalny, R., & Gente, P. (1996). Volcanic growth faults and the origin of Pacific abyssal hills. *Nature*, 380, 125–129.
- Masson, D. G. (1991). Fault patterns at outer trench walls. *Marine Geophysical Researches*, 13, 209–225. <https://doi.org/10.1007/BF00369150>

- Matulka, P., Wiens, D. A., Li, Z., Barcheck, G., Abers, G. A., & Ruppert, N. (2022). Along-strike Variation in Plate-bending Seismicity and Relationship to the Seismic Cycle in the Alaska Subduction Zone. *Seismological Research Letters*, 93, 1299 (abstract).
- Maus, S., Barckhausen, U., Berkenbosch, H., Bournas, N., Brozena, J., Childers, V., Dostaler, F., Fairhead, J. D., Finn, C., Von Frese, R. R. B., Gaina, C., Golynsky, S., Kucks, R., Lühr, H., Milligan, P., Mogren, S., Müller, R. D., Olesen, O., Pilkington, M., ... Tontini, F. C. (2009). EMAG2: A 2-arc min resolution Earth Magnetic Anomaly Grid compiled from satellite, airborne, and marine magnetic measurements. *Geochemistry, Geophysics, Geosystems*, 10, Q08005. <https://doi.org/10.1029/2009GC002471>
- Miller, N. C., Lizarralde, D., Collins, J. A., Holbrook, W. S., & Van Avendonk, H. J. A. (2021). Limited Mantle Hydration by Bending Faults at the Middle America Trench. *Journal of Geophysical Research: Solid Earth*, 126, e2020JB020982. <https://doi.org/10.1029/2020JB020982>
- Mortera-Gutiérrez, C. A., Scholl, D. W., & Carlson, R. L. (2003). Fault trends on the seaward slope of the Aleutian Trench: Implications for a laterally changing stress field tied to a westward increase in oblique convergence. *Journal of Geophysical Research*, 108(B10), 2477. <https://doi.org/10.1029/2001JB001433>
- Naliboff, J. B., Billen, M. I., Gerya, T., & Saunders, J. (2013). Dynamics of outer-rise faulting in oceanic-continental subduction systems. *Geochemistry, Geophysics, Geosystems*, 14(7), 2310–2327. <https://doi.org/10.1002/ggge.20155>

- Nishikawa, T., & Ide, S. (2015). Background seismicity rate at subduction zones linked to slab-bending-related hydration. *Geophysical Research Letters*, 42(17), 7081–7089. <https://doi.org/10.1002/2015GL064578>
- Obana, K., Fujie, G., Takahashi, T., Yamamoto, Y., Tonegawa, T., Miura, S., & Kodaira, S. (2019). Seismic velocity structure and its implications for oceanic mantle hydration in the trench-outer rise of the Japan Trench. *Geophysical Journal International*, 217(3), 1629–1642. <https://doi.org/10.1093/gji/ggz099>
- Ogawa, Y., Kobayashi, K., Hotta, H., & Fujioka, K. (1997). Tension cracks on the oceanward slopes of the northern Japan and Mariana Trenches. *Marine Geology*, 141, 111–123. [https://doi.org/10.1016/S0025-3227\(97\)00059-5](https://doi.org/10.1016/S0025-3227(97)00059-5)
- Peacock, S. M. (2001). Are the lower planes of double seismic zones caused by serpentine dehydration in subducting oceanic mantle? *Geology*, 29(4), 299–302. [https://doi.org/10.1130/0091-7613\(2001\)029<0299:ATLPOD>2.0.CO;2](https://doi.org/10.1130/0091-7613(2001)029<0299:ATLPOD>2.0.CO;2)
- Pérez-Gussinyé, M., Lowry, A. R., Phipps Morgan, J., & Tassara, A. (2008). Effective elastic thickness variations along the andean margin and their relationship to subduction geometry. *Geochemistry, Geophysics, Geosystems*, 9(2). <https://doi.org/10.1029/2007GC001786>
- Petersen, S. E., Hoisch, T. D., & Porter, R. C. (2021). Assessing the Role of Water in Alaskan Flat-Slab Subduction. *Geochemistry, Geophysics, Geosystems*, 22(5). <https://doi.org/10.1029/2021GC009734>
- Protti, M., Güendel, F., & McNally, K. (1994). Correlation between the age of the subducting Cocos plate and the geometry of the Wadati-Benioff zone under Nicaragua

988 and Costa Rica. *Physics of the Earth and Planetary Interiors*, 84, 271–287.

989 <https://doi.org/10.1130/SPE295-p309>

990 Ranero, C. R., Morgan, J. P., McIntosh, K., & Relchert, C. (2003). Bending-related faulting

991 and mantle serpentinization at the Middle America trench. *Nature*, 425, 367–373.

992 <https://doi.org/10.1038/nature01961>

993 Ranero, C. R., Villaseñor, A., Morgan, J. P., & Weinrebe, W. (2005). Relationship between

994 bend-faulting at trenches and intermediate-depth seismicity. *Geochemistry,*

995 *Geophysics, Geosystems*, 6(12), Q12002. <https://doi.org/10.1029/2005GC000997>

996 Ryan, W. B. F., Carbotte, S. M., Coplan, J. O., O’Hara, S., Melkonian, A., Arko, R.,

997 Weissel, R. A., Ferrini, V., Goodwillie, A., Nitsche, F., Bonczkowski, J., & Zemsky,

998 R. (2009). Global multi-resolution topography synthesis. *Geochemistry, Geophysics,*

999 *Geosystems*, 10(3). <https://doi.org/10.1029/2008GC002332>

1000 Saffer, D. M., & Tobin, H. J. (2011). Hydrogeology and mechanics of subduction zone

1001 forearcs: Fluid flow and pore pressure. *Annual Review of Earth and Planetary*

1002 *Sciences*, 39, 157–186. <https://doi.org/10.1146/annurev-earth-040610-133408>

1003 Saffer, D. M., & Wallace, L. M. (2015). The frictional, hydrologic, metamorphic and

1004 thermal habitat of shallow slow earthquakes. *Nature Geoscience*, 8(8), 594–600.

1005 <https://doi.org/10.1038/ngeo2490>

1006 Scanlon, K. M., & Masson, D. G. (1992). Fe-Mn nodule field indicated by GLORIA, north

1007 of the Puerto Rico Trench. *Geo-Marine Letters*, 12, 208–213.

1008 <https://doi.org/10.1007/BF02091840>

1009 Sella, G. F., Dixon, T. H., & Mao, A. (2002). REVEL: A model for Recent plate velocities
1010 from space geodesy. *Journal of Geophysical Research: Solid Earth*, 107(B4), ETG 11-
1011 1-ETG 11-30. <https://doi.org/10.1029/2000jb000033>

1012 Sharples, W., Jadamec, M. A., Moresi, L. N., & Capitanio, F. A. (2014). Overriding plate
1013 controls on subduction evolution. *Journal of Geophysical Research: Solid Earth*,
1014 119(8), 6684–6704. <https://doi.org/10.1002/2014JB011163>

1015 Shillington, D. J., Bécel, A., Nedimovic, M. R., Kuehn, H., Webb, S. C., Abers, G. A.,
1016 Keranen, K. M., Li, J., Delescluse, M., & Mattei-Salicrup, G. A. (2015). Link between
1017 plate fabric, hydration and subduction zone seismicity in Alaska. *Nature Geoscience*,
1018 8, 961–964. <https://doi.org/10.1038/ngeo2586>

1019 Smith, D. K., Schouten, H., Zhu, W. L., Montési, L. G. J., & Cann, J. R. (2011). Distributed
1020 deformation ahead of the Cocos-Nazca Rift at the Galapagos triple junction.
1021 *Geochemistry, Geophysics, Geosystems*, 12(11), Q11003.
1022 <https://doi.org/10.1029/2011GC003689>

1023 Stevenson, A. J., Scholl, D. W., & Vallier, T. L. (1983). Tectonic and geologic implications
1024 of the Zodiac fan, Aleutian Abyssal Plain, northeast Pacific. *Geological Society of*
1025 *America Bulletin*, 94, 259–273. [https://doi.org/10.1130/0016-](https://doi.org/10.1130/0016-7606(1983)94<259:TAGIOT>2.0.CO;2)
1026 [7606\(1983\)94<259:TAGIOT>2.0.CO;2](https://doi.org/10.1130/0016-7606(1983)94<259:TAGIOT>2.0.CO;2)

1027 Straume, E. O., Gaina, C., Medvedev, S., Hochmuth, K., Gohl, K., Whittaker, J. M., Abdul
1028 Fattah, R., Doornenbal, J. C., & Hopper, J. R. (2019). GlobSed: Updated Total
1029 Sediment Thickness in the World’s Oceans. *Geochemistry, Geophysics, Geosystems*,
1030 20, 1756–1772. <https://doi.org/10.1029/2018GC008115>

1031 Triezenberg, P. J., Hart, P. E., & Childs, J. R. (2016). *National Archive of Marine Seismic*
 1032 *Surveys (NAMSS): A USGS data website of marine seismic reflection data within the*
 1033 *U.S. Exclusive Economic Zone (EEZ): U.S. Geologic Survey Data Release.*

1034 Van Avendonk, H. J. A., Holbrook, W. S., Lizarralde, D., & Denyer, P. (2011). Structure
 1035 and serpentinization of the subducting Cocos plate offshore Nicaragua and Costa Rica.
 1036 *Geochemistry, Geophysics, Geosystems*, 12(6). <https://doi.org/10.1029/2011GC003592>

1037 Van Keken, P. E., Hacker, B. R., Syracuse, E. M., & Abers, G. A. (2011). Subduction
 1038 factory: 4. Depth-dependent flux of H₂O from subducting slabs worldwide. *Journal of*
 1039 *Geophysical Research: Solid Earth*, 116, B01401.
 1040 <https://doi.org/10.1029/2010JB007922>

1041 von Huene, R., Miller, J. J., & Weinrebe, W. (2012). Subducting plate geology in three
 1042 great earthquake ruptures of the western Alaska margin, Kodiak to Unimak.
 1043 *Geosphere*, 8(3), 628–644. <https://doi.org/10.1130/GES00715.1>

1044 Wang, K., & Bilek, S. L. (2014). Invited review paper: Fault creep caused by subduction of
 1045 rough seafloor relief. *Tectonophysics*, 610, 1–24.
 1046 <https://doi.org/10.1016/j.tecto.2013.11.024>

1047 Wei, S. S., Ruprecht, P., Gable, S. L., Huggins, E. G., Ruppert, N., Gao, L., & Zhang, H.
 1048 (2021). Along-strike variations in intermediate-depth seismicity and arc magmatism
 1049 along the Alaska Peninsula. *Earth and Planetary Science Letters*, 563, 116878.
 1050 <https://doi.org/10.1016/j.epsl.2021.116878>

1051 Worthington, L. L., Van Avendonk, H. J. A., Gulick, S. P. S., Christeson, G. L., & Pavlis,
 1052 T. L. (2012). Crustal structure of the Yakutat terrane and the evolution of subduction

and collision in southern Alaska. *Journal of Geophysical Research: Solid Earth*, 117, B01102. <https://doi.org/10.1029/2011JB008493>

Xiao, Z., Freymueller, J. T., Grapenthin, R., Elliott, J. L., Drooff, C., & Fusso, L. (2021). The deep Shumagin gap filled: Kinematic rupture model and slip budget analysis of the 2020 Mw 7.8 Simeonof earthquake constrained by GNSS, global seismic waveforms, and floating InSAR. *Earth and Planetary Science Letters*, 576, 117241. <https://doi.org/10.1016/j.epsl.2021.117241>

Yang, L., Wang, J., & Xu, C. (2023). Coseismic Coulomb stress changes induced by a 2020–2021 MW > 7.0 Alaska earthquake sequence in and around the Shumagin gap and its influence on the Alaska-Aleutian subduction interface. *Geodesy and Geodynamics*. <https://doi.org/10.1016/j.geog.2023.04.007>

Zhao, B., Bürgmann, R., Wang, D., Zhang, J., Yu, J., & Li, Q. (2022). Aseismic slip and recent ruptures of persistent asperities along the Alaska-Aleutian subduction zone. *Nature Communications*, 13(3098). <https://doi.org/10.1038/s41467-022-30883-7>

Zhou, Y., Wang, W., He, J., Wang, X., Pan, Z., & Zhao, G. (2022). The 19 October 2020 Mw 7.6 Earthquake in Shumagin, Alaska: An Unusual Dextral Strike-Slip Event. *Pure and Applied Geophysics*, 179, 3527–3542. <https://doi.org/10.1007/s00024>